TU Delft University

CRAB

Development of a Tendon-Driven Robotic Device with Soft Flexible Wheels for Mobility on Biofouled Subsea Pipelines

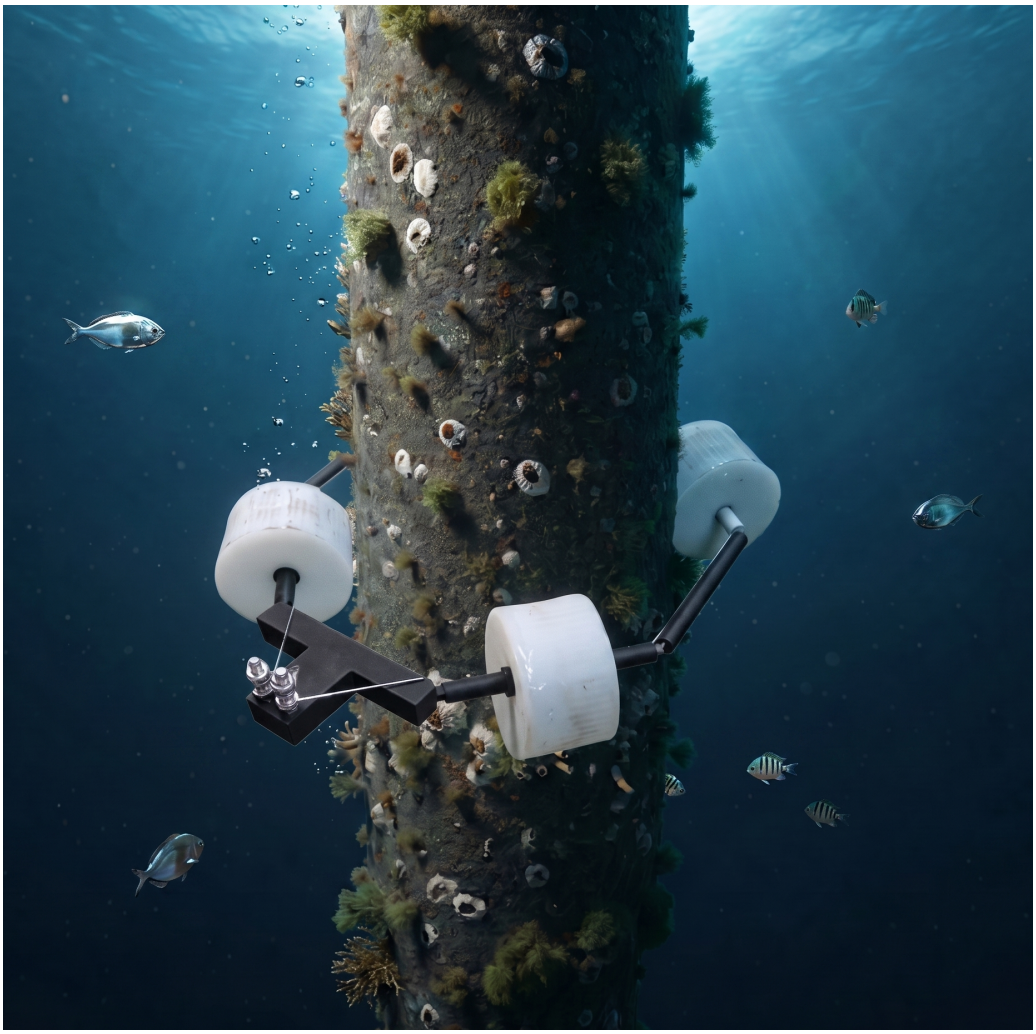

Robert Geerts

May 13, 2026

Abstract

The autonomous inspection of subsea infrastructure is significantly hindered by marine biofouling, which frequently causes traditional rigid crawlers to stall or necessitates expensive, time-consuming surface cleaning. Furthermore, the subsea infrastructure itself introduces significant obstacles, as the path is frequently interrupted by geometrically complex architectures such as interconnected valve assemblies, flanges or varying pipeline diameters. To address these limitations, this research presents the design, computational modelling, and empirical validation of the Compliant Robotic Architecture for Biofouling (CRAB) prototype. The CRAB leverages inherent material compliance to overcome these obstacles on pipelines.

The architecture integrates three core subsystems: a tendon-driven, underactuated gripper for adaptive enclosure, a passive magnetic sliding track for variable circumference locking, and fluid-filled flexible wheels designed to deform over obstacles. Finite element analysis was utilised to optimise the wheel morphology.

Empirical validation of the prototype confirmed the viability of the core design concept, with the CRAB successfully achieving a secure grasp and overcoming simulated radial biofouling up to 50 mm in radius. However, testing also exposed critical failures, specifically material ruptures at 60 mm obstacle and kinematic stalling within the variable locking mechanism.

Ultimately, this research validates the foundational methodology of using passive mechanical compliance for unstructured subsea mobility. While the core kinematics are proven effective, advancing the system toward autonomous field deployment requires the integration of an active mobility actuation system, comprehensive dynamic stability analysis, structural refinements and material optimisation.

Keywords: *Soft Robotics, Subsea Mobility, Passive Compliance, Obstacle Traversal, Tendon-Driven Gripper, Marine Biofouling, Flexible Wheels.*

CONTENTS

1. Introduction

1.1. Background

Worldwide, significant investments are currently being made to accelerate the global energy transition [1]. This shift has driven a rapid expansion of offshore wind farms and their subsea cable networks [2]. To meet the rising demand for green power and achieve international climate goals, these infrastructure projects are increasingly being developed further offshore and in deeper, more challenging waters [3] [4]. The kilometres of underwater cables form the backbone and lifelines of our modern, international energy grids [4]. They bridge the gap between offshore wind generation and the mainland, while simultaneously linking the electricity networks of neighbouring countries.

Beyond the energy sector, the demand for resilient subsea infrastructure extends to several other global stakeholders. The telecommunications industry manages a vast network of fibre optic data cables vital for international connectivity [5], while oil and gas companies maintain extensive pipeline infrastructure [6]. While this report frequently uses the term 'pipes' to describe this architecture, it is important to note that the kinematics are equally applicable to subsea power cables, telecommunication lines, and other tubular marine structures. These structures present the identical mechanical challenge of a cylindrical profile. Furthermore, safeguarding these underwater assets against hybrid threats and sabotage has become a national defensive strategic priority [7]. Across all these sectors, these crucial components are continuously subjected to harsh environmental stressors [8]. As this underwater infrastructure ages, the risks of undetected wear, tear, and material fatigue increase exponentially. The unexpected failure of a primary subsea cable or pipeline not only incurs significant repair costs, but it also actively compromises the energy and data security of entire regions [4]. Consequently, the necessity for reliable, proactive, and advanced structural inspections is critical to prevent failures, extend operational lifespans, and ensure long-term economic stability [1].

Executing these proactive maintenance and inspection operations, however, presents a profound engineering challenge [9]. The operational integrity of these networks relies on navigating underwater environments characterised by extreme structural heterogeneity. A typical subsea network is not a uniform landscape; rather, it comprises an intricate array of elements of vastly differing diameters. Furthermore, the path is frequently interrupted by geometrically complex architectures such as interconnected valve assemblies and irregular flanges [10]. This inherent structural diversity dictates that any automated inspection vehicle must possess the kinematic flexibility to adapt to drastically different topographies within a single deployment.

Crucially, this baseline geometric complexity is compounded by the rapid and unpredictable accumulation of marine biofouling [11]. Over time, submerged infrastructure is colonised by a variety of marine organisms, ranging from soft sponges and algae to hard, calcified structures such as barnacles, mussels, and tubeworms. This biological growth fundamentally alters the original, predictable geometry of the manufactured components, introducing random, macroscopic protrusions and obstacles along the surface [11].

Consequently, automating the inspection and repair of these critical lifelines requires a novel robotic device [4]. The primary engineering challenge lies in developing a system capable of continuously traversing both designed architectural variations and the unpredictable hurdles of marine biofouling, all without experiencing mechanical stalling.

1.2. State of the art

Meeting these severe environmental challenges requires moving beyond the limitations of existing commercial devices. Standard external subsea crawlers are generally engineered for operation on rigid, uniform surfaces [9], [12]. These systems typically utilise rigid drive mechanisms that lack the mechanical compliance required to accommodate significant variations in pipe diameters. Because these robots rely on precise surface contact for traction, they are highly sensitive to the lack of standardisation in subsea infrastructure. A critical failure point for existing robotic devices is the presence of biological fouling; the irregular and hard protrusions created by organisms such as barnacles and coral present a high risk of mechanical

stalling or total entrapment for rigid drive systems.

To navigate subsea pipes while maintaining continuous motion, integrated "clean-and-traverse" subsea robots represent a specialised class of inspection vehicles that overcome heavily fouled marine environments by actively stripping away biofouling immediately ahead of their path [13], [14]. This sequential methodology is critical because diverse robotic mobility mechanisms strictly require an unobstructed, uniform surface to function properly [13], [14]. For instance, rigid mechanised systems like the Roto Climber (Figure 1.1) must clear thick marine growth so their motorised wheels can physically grip the underlying surface without slipping, while thruster-driven, positively buoyant systems like the AURI (Autonomous Underwater Riser Inspection Tool) rely on a freshly cleaned cylindrical profile to maintain precise structural alignment using unpowered guide wheels [13], [14]. Furthermore, this aggressive pre-traversal surface preparation carries high operational and environmental costs. Technically, the abrasive mechanical force required to strip hard, calcified biofouling physically damages the pipe's vital anti-corrosion coatings [15]. This exposes the vulnerable steel to highly oxygenated seawater and surviving sulfate-reducing bacteria, severely accelerating localised degradation such as pitting and microbially influenced corrosion (MIC). Environmentally, the eradication of this growth systematically strips away localised biomass, destroying the micro-ecosystems that have come to rely on the underwater infrastructure as an artificial reef.

While external inchworm subsea pipe crawlers (Figure 1.2) avoid aggressively destroying marine growth, their step-by-step mobility introduces severe operational drawbacks, most notably their slow speed [16], [17], [18]. The peristaltic "clamp, extend, and pull" motion is inherently sluggish, making the inspection of long subsea pipes highly time consuming and heavily draining on power reserves due to the constant mechanical actuation. Furthermore, because these robots do not strip the pipe clean, they frequently suffer from grip failure and slippage when trying to clamp over thick, slippery biofouling. Ultimately, the sheer mechanical complexity required to operate alternating hydraulic or pneumatic clamping systems in the high-pressure deep-ocean environment introduces numerous potential points of failure, making inchworm crawlers prone to failures [16], [18].

While soft robotic research has extensively explored adaptive enclosure, most systems remain optimised for static manipulation, securing objects in a fixed position [19]. Consequently, a significant technological gap exists in leveraging material compliance to achieve robust, bidirectional mobility in unstructured subsea environments. By bridging this gap, such an architecture could bypass the rigid limitations of traditional crawlers. Ultimately, this could lead to a unified, highly efficient solution where the severe structural and environmental costs of aggressively stripping marine growth and the operational inefficiency of the inchworm's slow speed are all simultaneously resolved.

Figure 1.1: Roto climber.

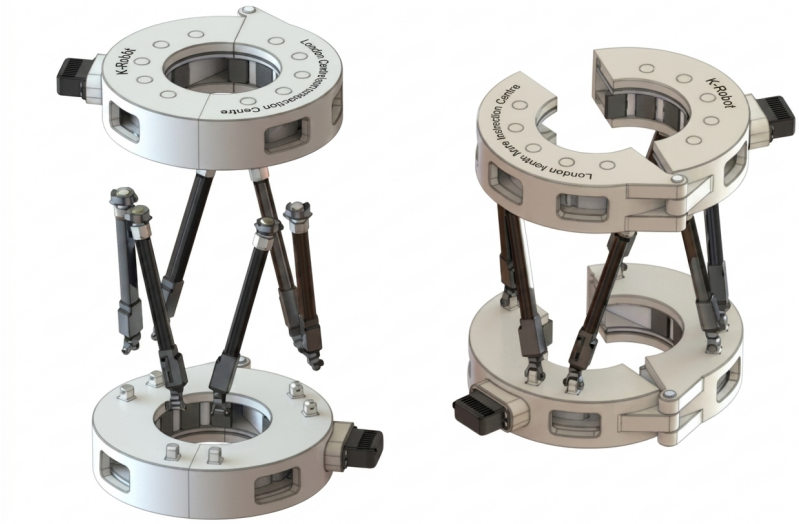

Figure 1.2: Inchworm.

1.3. OBJECTIVE

Main Research Goal: *Develop an adaptive underwater robotic mobility device to overcome the geometric irregularities and biological unpredictability inherent in subsea infrastructure.*

Sub questions: To answer the main research question, the following sub-questions will be addressed:

- How can the behavioural requirements of gripping, variable circumference locking and obstacle handling be resolved through the selection of robotic subsystems?
- How can these discrete subsystems be physically integrated to function as a unified, Compliant Robotic Architecture for Biofouling (CRAB) device?
- How does the geometric dimensioning of a fluid-filled flexible wheel affect its behaviour and stability when interacting with obstacles?
- What operational capabilities does the unified robotic device demonstrate, and what key lessons can be drawn from the empirical case studies?

1.4. STRUCTURE OF THE THESIS

To answer the formulated research questions and systematically develop the adaptive underwater device, this thesis is structured as follows:

- *Chapter 2:* Breaks down the overarching behavioural requirements into discrete kinematic tasks. It details the conceptualisation, systematic evaluation using a morphological map, and empirical validation of the three primary robotic subsystems: gripping, the variable circumference locking and the obstacle handling.
- *Chapter 3:* Discusses the physical and kinematic integration of these discrete mechanisms into a unified, functional robot designated as CRAB. It outlines the strict geometric compatibility, the dynamic kinematic coupling between the compliant wheels and the magnetic slider, macroscopic system stability, and the fabrication methodology of the physical proof-of-concept.
- *Chapter 4:* Isolates the flexible wheel subsystem to investigate its non-linear deformation mechanics using Finite Element Analysis (FEA). It covers the computational modelling and empirical calibration of the FEA framework. Then it presents a quantitative analysis of the wheel's structural forces and dynamic kinematic responses during obstacle handling.
- *Chapter 5:* This chapter presents the experimental testing of the unified CRAB prototype. It details the setups used, evaluates the system's operational capabilities in grasping, variable circumference locking and obstacle handling. Then it critically analyses the physical failures, such as material ruptures and kinematic binding, exposed during extreme mechanical loading.
- *Chapter 6:* The final chapter synthesises the theoretical and empirical findings to directly answer the overarching research questions. It acknowledges the current methodological and structural limitations and outlines targeted recommendations for future development.

2. SUBSYSTEM DESIGN AND EVALUATION

The transition from a theoretical concept to a functional robotic device requires a decomposition of the subsea mobility challenge into discrete, manageable kinematic tasks. While the previous chapter established the environmental stressors, namely geometric heterogeneity and marine biofouling, this chapter focuses on the mechanical architecture required to navigate them.

Section 2.1 defines the essential behavioural requirements derived directly from the physical challenges of the subsea operational environment. To systematically generate and evaluate potential solutions for these requirements, Section 2.2 introduces a morphological map. The subsequent sections detail the theoretical evaluation and physical prototyping of the three primary subsystems: the variable circumference locking (Section 2.3), the gripping (Section 2.4), and the obstacle handling (Section 2.5). Finally, Section 2.6 discusses the outcomes and findings of the subsystem design and evaluation.

2.1. BEHAVIOURAL REQUIREMENTS

The behavioural requirements are derived from the operational challenges of the subsea environment and from the specific technical needs for handling subsea infrastructure.

- **Gripping:** The gripping subsystem is designed to accommodate structural diameters of 300 mm. This boundary was selected because 300 mm is a dimension commonly encountered throughout subsea infrastructure [10].
- **Obstacle handling:** The system must traverse up to 50 mm of radial marine growth without mechanically stalling. This specific threshold was established to simulate severe, mature accumulation of biofouling encountered on infrastructure [11].
- **Variable circumference locking:** The mechanism must securely lock around the subsea infrastructure, while dynamically adapting its internal circumference to accommodate varying structural diameters or to negotiate uneven marine growth.

Because subsea pipes vary greatly in size, these target dimensions give us a clear range for testing. Setting these boundaries allows us to validate that the robot's mechanics and flexibility work as intended. While this report focuses heavily on navigating obstacles like marine growth, the flexibility required to roll over those bumps is similar to the mechanical flexibility needed to adjust to different pipe diameters, valves and flanges. Ultimately, proving the robot works within this specific size range creates a strong proof of concept that can be scaled to other pipes and obstacles in the future.

2.2. MORPHOLOGICAL MAP:

To synthesise mechanisms capable of executing the defined behavioural requirements, a morphological map (Table 2.1) was generated to systematically evaluate potential architectural solutions for each discrete kinematic task. However, because the device must operate as a highly coupled dynamic system, subsystem compatibility serves as a primary analytical criterion; the selected mechanisms must integrate without kinematic interference. Furthermore, while continuous mobility and payload integration fall outside the primary scope of this initial prototyping phase, any selected architecture must ensure these integrations remain possible for a later stage of development.

Gripping	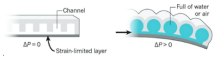 Fluidic	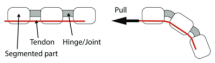 Tendon	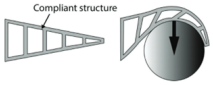 Compliant	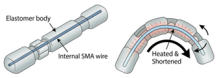 SMA
Obstacle handling	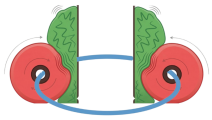 Flexible wheels	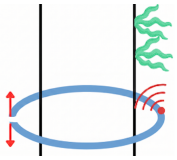 Sensors	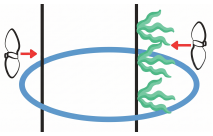 Propellers	
Variable circumference locking	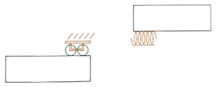 Velcro	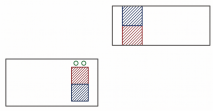 Magnet	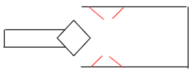 Compliant	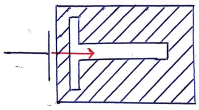 Mechanical

Table 2.1: Morphological evaluation of potential robotic subsystems. This map systematically breaks down architectural solutions for each discrete kinematic task. To ensure a functional final prototype, the selected mechanisms had to prove not only individual viability for gripping, obstacle handling, and locking, but strict system-level compatibility and allow for mobility and payload integration.

2.3. Variable Circumference Locking Mechanism

To satisfy the behavioural requirement of variable circumference locking, the robotic device requires a locking mechanism that allows the system to adapt its internal circumference to accommodate variable diameters without decoupling.

2.3.1. Morphological Evaluation

To identify the most viable architecture for variable diameter environments, potential mechanisms were evaluated against the required kinematic behaviours:

- **Micro-structured Fasteners (Velcro):** This concept utilises micro-structured fasteners on a sliding rail system. Despite successful use in highly controlled underwater applications [20], hook-and-loop fasteners are behaviourally unsuited for subsea deployment. Their high-surface-area matrix is immediately vulnerable to rapid marine biofouling, which destroys interfacial shear strength [20]. Additionally, establishing a reliable bond requires applying a uniform normal force to expel the viscous water layer [21].
- **Mechanical Locks:** This system utilises a slotted track mechanism where a locking rod enters through a specifically aligned opening. Once inserted and translated laterally along the track, the rod becomes physically trapped and cannot disengage unless returned to its original entry point. While this effectively locks the system while preserving one translational degree of freedom, it requires high precision in the coupling process. Achieving this high-precision initial coupling is inherently unreliable when subjected to unpredictable hydrodynamic forces [22]. Mechanical locks are uniquely vulnerable because they rely on tight tolerances and sliding interfaces to remain secure. In a subsea environment, sand, silt, and biofouling act as an abrasive "grit" that fills the small gaps required for pins or tracks to move.
- **Compliant Systems:** The compliant system has a funnel-shaped entry with compliant locking components. While this design effectively eliminates jam prone moving parts, designing a compliant interface that supports dynamic circumference adjustments while ensuring reliable decoupling introduces substantial kinematic complexity and risks of cyclic material fatigue [23].

- **Magnetic Locking:** This concept utilises magnetic attraction to facilitate closure, integrated with a linear rail system to provide a translational degree of freedom. Within this paradigm, both active electromagnets and passive permanent magnets were evaluated. While electromagnets theoretically offer the advantage of on-demand, switchable engagement, their implementation introduces significant architectural complexities. Utilising active magnetic systems necessitates continuous power routing along the articulating joints and the integration of dedicated electrical switching hardware. Conversely, passive permanent magnets provide a reliable holding force that is entirely independent of power reserves.

Subsea environmental constraints, specifically unpredictable hydrodynamic forces, disqualified microstructured fasteners and mechanical locks due to their reliance on high-precision alignment and uniform attachment force, favouring instead the passive alignment offered by permanent magnets and compliant funnels.

2.3.2. Empirical validation

To physically validate the theoretical advantages of the surviving concepts, prototype iterations of both the magnetic slider (Figure 2.1) and the compliant funnel (Figure 2.2) were developed and tested.

The sliding rail effectively executed the necessary translational degree of freedom, providing low friction movement and highly effective passive self alignment. Conversely, the alternative compliant funnel proved structurally fragile.

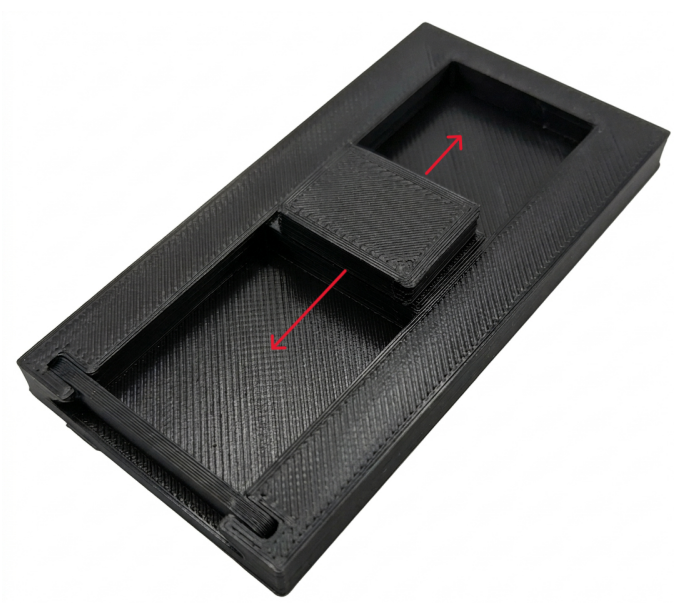

Figure 2.1: Prototype of the magnetic sliding mechanism, which successfully demonstrated low-friction, passive self-alignment. The 80x40 mm assembly utilises a base slider within linear guide rails and integrated permanent magnets. The red arrows indicate the system's translational path.

Figure 2.2: The structurally fragile compliant funnel prototype. This 60x100 mm assembly relies on an arrow-shaped rod pushing past flexible internal latches to lock. translating along the path indicated by the red arrows.

2.4. Gripping

To fulfil the behavioural requirement of gripping, specifically, the ability to adaptively enclose infrastructure up to 300 mm in diameter, the grasping mechanism must exhibit both high scalability and a rapid closing trajectory.

2.4.1. Morphological evaluation

To determine the optimal actuation behaviour, gripping technologies were evaluated against the system's spatial and kinematic constraints:

- **Fluidic Actuators:** While highly effective for centimetre scale manipulation, fluidic elastomer actuators lack practical scalability for a 300 mm target [19]. Because the internal volume of fluidic chambers scale cubically with its linear dimensions, achieving the necessary wrap would require massive volumetric flow rates. This behavioural constraint necessitates bulky compressors, which violates the requirement for a compact, hydrodynamically efficient device [19].
- **Shape Memory Alloys (SMA):** The low recoverable strain of SMAs (typically 6% to 10%) fundamentally restricts their kinematic range [24]. Achieving the required 300 mm stroke would demand excessively long wires or heavy mechanical amplification, actively undermining the system's spatial efficiency.
- **Deformation-Based Grippers:** Systems utilising continuous material deformation inherently adapt to any geometric variation they encounter [25], [26]. For a device navigating a fouled subsea pipe, this behaviour is highly problematic; the gripper will attempt to conform to unpredictable biological obstructions rather than maintaining a stable perimeter around the cylindrical profile, likely resulting in mechanical stalling.
- **Tendon-Driven Systems:** Tendon-driven systems operate through tension-induced bending, where a high-tensile line is routed through structural links and elastic flexure joints. Applying tension to this line creates a compressive moment at each joint, forcing the arm to curl. This underactuated architecture offers inherent scalability and morphological adaptability, enabling the arms to passively conform to various geometries while maintaining high-force mechanical constraints. By centralising actuation, the system maintains a slim, low-profile geometry. Furthermore, the design achieves kinematic simplicity, as the wrapping trajectory is governed by joint stiffness rather than complex active control, reducing potential electrical and mechanical failure points [27].

Consequently, because alternative actuators fail to scale to the required 300 mm enclosure or are prone to mechanical stalling, the tendon-driven system is the only viable option to achieve the necessary gripping.

2.4.2. Empirical validation

Initial empirical evaluations of the baseline tendon mechanism revealed kinematic deviations from the targeted circular enclosure (Figure 2.3). Consequently, to optimise the joint trajectory and systematically analyse the wrapping mechanics, subsequent prototypes were developed to evaluate the structural behaviour of three-, four-, and six-link configurations (Figure 2.4).

The multi-link gripper configurations were empirically tested by incrementally applying tension to the primary actuation tendon and visually analysing the resulting wrapping trajectory. These observational trials revealed a fundamental kinematic trade-off regarding the number of links used:

- **The advantage of more links:** Increasing the number of structural links creates more degrees of freedom within the system. Theoretically, this enables the gripper to achieve a higher-resolution, which can result in a more continuous enclosure around circular diameters.
- **The disadvantage of more links:** However, these compounding degrees of freedom introduce significant non-linearity into the grasping motion, degrading the predictability of the wrap.

This unpredictability stems directly from the system's inherently underactuated architecture. Because a single tendon drives multiple flexures, the system possesses fewer control inputs than degrees of freedom. Consequently, the wrapping trajectory is governed by the relative stiffness of individual joints rather than rigid kinematics. Compounding these unactuated joints exponentially amplifies this non-linear behaviour, making a synchronised, circular wrap mechanically difficult to guarantee.

To optimise this trade-off between kinematic simplicity and the spatial demands of a circular enclosure, the final design converged on a three-link, two-flexure configuration. By incorporating pre-angled geometries into the central and terminal links rather than relying strictly on linear segments, the arms effectively

Figure 2.3: First gripper prototype, with an overall arm length of 300 mm.

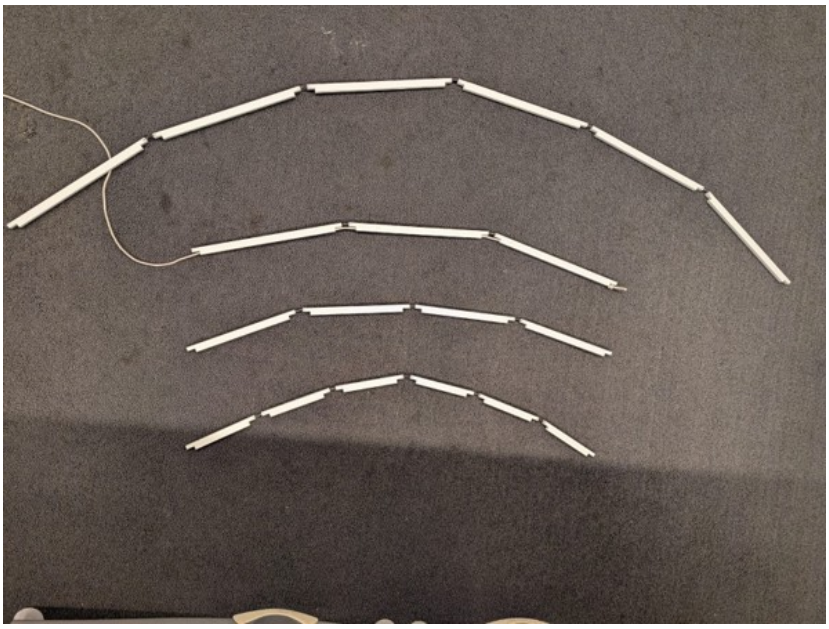

Figure 2.4: Multi-link gripper prototypes evaluating the trade-off between resolution and predictability. These configurations range from 900 mm to 1800 mm arm lengths.

approximate a circular perimeter without the control overhead and instability of additional joints (shown in Figures 2.5 and 2.6). Figure 2.7 shows the incorporation of the magnet slider in the most closed configuration.

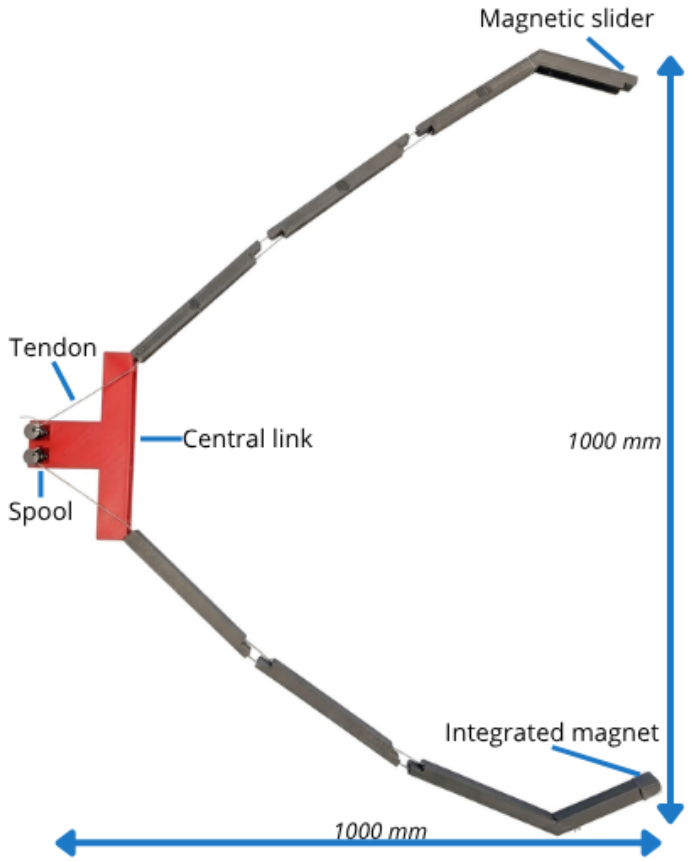

Figure 2.5: This 1000x1000 mm third-iteration gripper uses three pre-angled, spool-actuated links to achieve a predictable circular wrap without the instability of extra joints.

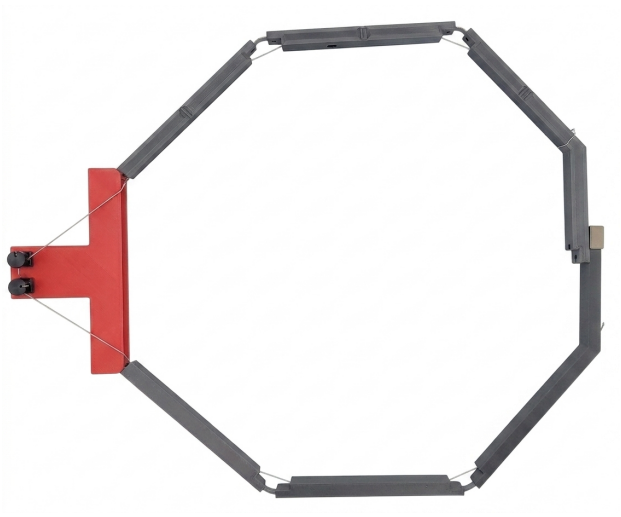

Figure 2.6: 600x500 mm integrated prototype in a fully closed state. This configuration illustrates the mechanical synergy between the tendon arms and the magnetic slider. It demonstrates that the system can maintain a magnetically coupled enclosure

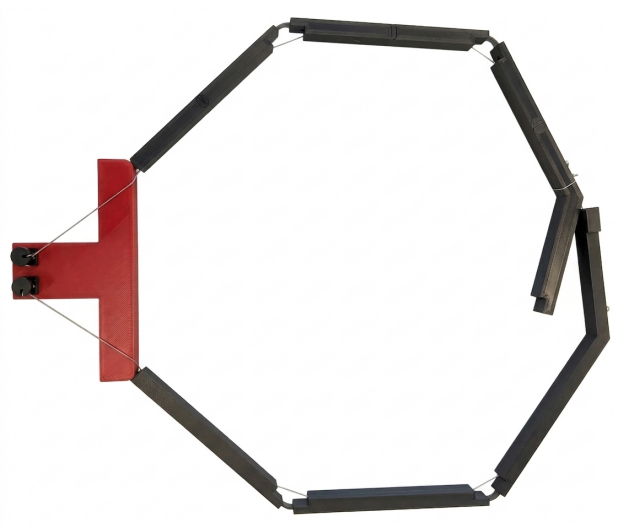

Figure 2.7: The magnetic slider at its maximum travel. This fully closed configuration demonstrates how the system accommodates varying structural circumference; the sliding mechanism allows the gripper to adjust its internal circumference without decoupling.

2.5. Obstacle handling

To maintain continuous vertical mobility, the device must successfully overcome the geometric unpredictability of the subsea environment. The accumulation of marine biofouling introduces drastic surface variations ranging from hard, sharp barnacle clusters to thick, slippery algae that pose a significant mechanical risk. Therefore, the mobility interface requires a mechanism capable of safely traversing these diverse and irregular protrusions without stalling, slipping, or entangling.

(a) Severe biofouling on a submerged pipe.

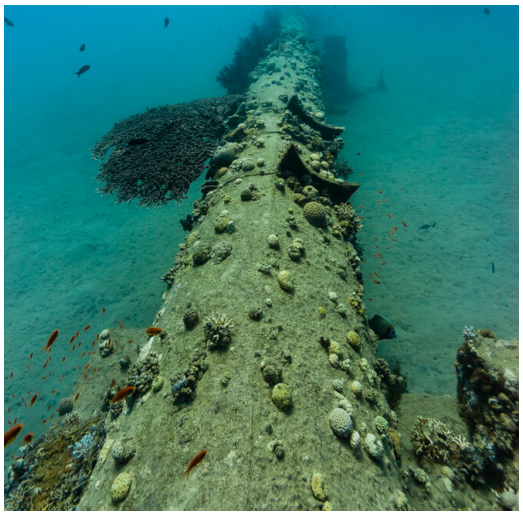

(b) Slight biofouling on a submerged pipe.

Figure 2.8: Examples of biofouling on pipes.

2.5.1. Morphological evaluation

To identify the most viable method for bypassing marine growth, three primary behavioural strategies were evaluated against the system's kinematic and environmental constraints:

- **Angled propellers:** This active strategy utilises propellers aimed directly along the device's path of travel. As the robot approaches an irregular protrusion, the thrusters direct a localised flow of water against the obstacle, creating a reactive hydrodynamic force intended to push the chassis safely away. However, this approach introduces two severe mechanical drawbacks. First, the repulsive thrust vector directly opposes the device's forward mobility, actively counteracting its own momentum. Second, the substantial integrated payload significantly increases the total mass of the chassis. Due to this high inertia, the physical response time required to quickly divert the heavy device is inherently slow. Generating sufficient force to overcome this inertia before impact would demand massive, instantaneous power spikes, rendering this strategy energy-inefficient and highly vulnerable to collisions.
- **Sensor triggered deployment:** By utilising integrated proximity sensors, the onboard control system continuously monitors the infrastructure's surface ahead. Upon detecting a protrusion within a critical distance threshold, the system actively opens its arms, temporarily expanding the circumference of the device to clear the hazard. However, the fundamental kinematic limitation of this design is that opening the enclosing arms does not alter the trajectory of the main chassis. If an obstacle lies directly in line with the central body, the device remains on a collision course, leaving the vehicle physically blocked despite the arms successfully deploying.
- **Flexible wheels:** This strategy provides inherent passive adaptability. By utilising highly compliant internal media, the wheels can dynamically deform around irregular protrusions without requiring complex active control systems or sensor feedback loops.

Since it requires no active evasion controls and lacks the situational vulnerabilities that leave alternative mechanisms prone to stalling, the passive flexible wheel was deemed the most viable solution.

2.5.2. Empirical validation

Unlike terrestrial pneumatic tyres, which are rendered unviable by the extreme hydrostatic pressures of the deep sea, the proposed flexible wheels must utilise pressure-invariant internal media to ensure structural integrity. To empirically validate the optimal physical behaviour, testing was structured around evaluating different internal media and iteratively refining the membrane material.

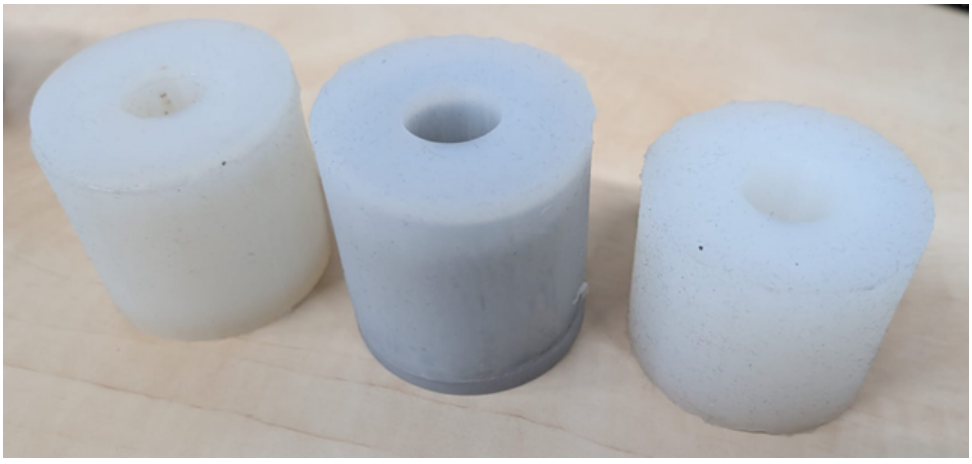

Figure 2.9: Flexible wheel prototypes with varying internal media, measuring approximately 60 mm in diameter and 60 mm in height. From left to right: water-filled, granular-filled, and solid silicone variants.

To determine the most efficient method for traversing obstacles, three distinct internal media concepts were initially prototyped using Dragon Skin 30 silicone (Figure 2.9), a material selected for its suitability in rapid prototyping and immediate availability within the TU Delft Phantom lab. The variants evaluated three primary paradigms of incompressible soft-body deformation:

- **Solid Silicone:** Evaluated the natural elasticity and deformation mechanics of a homogeneous silicone core when encountering radial obstacles.

- **Water Filled:** Investigated how an internal, incompressible fluid displaces to allow the outer membrane to smoothly conform to irregular protrusions.
- **Granular Filled:** Examined whether the friction between loose particulates (a 50/50 mixture of 2 mm and 3 mm stainless steel spheres) could effectively balance surface compliance with load-bearing strength.

During initial testing, the solid silicone Dragon Skin 30 prototype proved insufficiently flexible to effectively deform around the obstacles in Figure 2.10. To address this lack of compliance, a secondary solid prototype was fabricated using Ecoflex 00-30, a significantly softer silicone. While this alternative provided the necessary flexibility for obstacle handling, its low shore hardness made the wheel surface highly susceptible to tearing and abrasive wear. Consequently, relying purely on a solid elastomer, whether durable but stiff (Dragon Skin 30) or flexible but fragile (Ecoflex 00-30), forced an unacceptable compromise, rendering solid media unviable.

During comparative empirical testing using the setup shown in Figure 2.10, both the water- and granular-filled wheels exhibited identical traversal capabilities, stalling at the same maximum obstacle height and requiring equivalent force to navigate smaller protrusions. However, the granular medium, consisting of stainless steel ball bearings, introduces significant operational penalties, as it is substantially heavier and more costly than water. Consequently, water is the preferred internal medium.

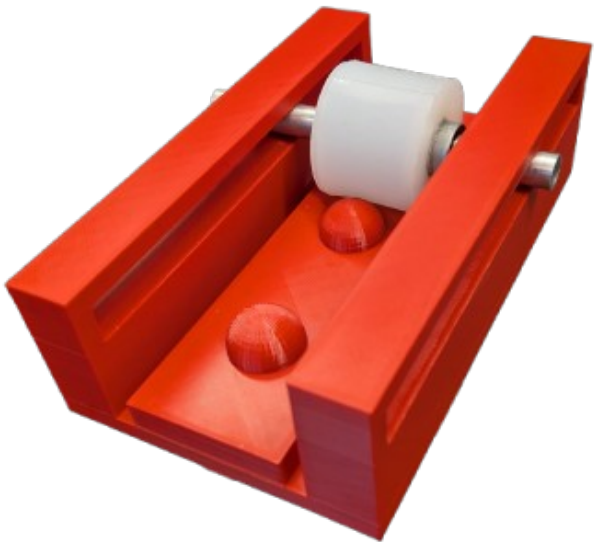

Figure 2.10: Empirical test setup evaluating wheels (from Figure 2.9) conforming over 15, 16, and 17 mm rigid obstacles. These trials confirmed that water-filled and granular-filled variants exhibited identical stalling thresholds.

2.6. Discussion

The primary objective of this chapter was to identify and validate discrete robotic subsystems capable of satisfying the core behavioural requirements. To directly address the sub-question regarding how the behavioural requirements of gripping, variable circumference locking, and obstacle handling can be resolved, this research concludes that the optimal architecture prioritises passive mechanical compliance and kinematic simplicity over active control. Specifically, these operational requirements are successfully resolved through the selection of the following three subsystems:

Regarding the gripping subsystem, the empirical trials demonstrated a fundamental trade-off between geometric resolution and kinematic predictability. The final choice converged on a tendon-driven, three-link, two-flexure configuration. While adding more links can theoretically improves the circular wrap, the empirical tests proved that compounding the unactuated degrees of freedom makes the system too unpre-

dictable. The chosen three-link design successfully balances the spatial flexibility needed to enclose 300 mm infrastructure with predictable actuation.

For the variable circumference locking requirement, the final choice prioritised passive magnetic coupling over compliant mechanical latches. While compliant funnels demonstrated theoretical promise, empirical testing revealed they were structurally fragile. The permanent magnetic sliding lock, conversely, provided highly reliable, low-friction dynamic coupling with passive alignment. Furthermore, utilising passive permanent magnets rather than electromagnets deliberately eliminated the architectural overhead of (waterproof) electronics, keeping the prototype focused strictly on validating mechanical kinematics.

To satisfy the obstacle handling requirement, water-filled flexible wheels were chosen over granular-filled or solid elastomer alternatives. Empirical testing established that relying on the volumetric displacement of an incompressible fluid offered continuous passive compliance over unpredictable biofouling, successfully conforming around different sizes of obstacles. These three subsystems successfully fulfil the foundational kinematic requirements for the CRAB prototype.

While the current prototype demonstrates the foundational kinematics, transitioning the architecture for field deployment introduces potential limitations. Although the water-filled wheels provided a functional baseline for compliance, the low-viscosity fluid lacks inherent passive damping. A theoretical concern is that high-velocity impacts with sharp biofouling could cause rapid fluid displacement, leading to the risk of the silicone bottoming out against the rigid axle and rupturing. To address this, future iterations might explore utilising non-Newtonian shear-thickening fluids (STFs) to improve impact damping. Additionally, while permanent magnets provided a reliable mechanical proof-of-concept, future models could incorporate switchable electromagnets to allow for on-of demand engagement. With the foundational subsystems now validated, the following chapter details their physical integration into the unified CRAB architecture.

3. CRAB

Building upon the isolated subsystem evaluations conducted in Chapter 2, this chapter details the physical and kinematic integration of these mechanisms into a unified robotic device. This fully integrated prototype is designated as CRAB: Compliant Robotic Architecture for Biofouling.

While the previous chapter validated the individual principles of variable circumference locking, soft gripping, and passive obstacle handling, these discrete systems must operate synergistically to achieve continuous mobility. This chapter outlines the engineering methodology used to synthesise these components into the complete CRAB architecture. Section 3.1 defines the strict geometric compatibility and spatial constraints required to merge the subsystems. Section 3.2 details the dynamic kinematic coupling between the compliant wheels and the magnetic sliding lock during obstacle handling. Section 3.3 analyses the macroscopic physical stability of the device. Next, Section 3.4 presents the fabrication methodology and material realisation of the physical proof-of-concept. Finally, Section 3.5 discusses the assembled CRAB prototype.

3.1. Geometry compatibility subsystems

The spatial integration of the discrete subsystems determines how well the robot handles different pipe sizes. The architecture is designed to lock around diameters of 300 mm to 400 mm. This 400 mm upper limit accounts for the 300 mm base pipe plus 50 mm of biofouling on each side.

Successful adaptability relies on a geometric equilibrium between three primary variables:

1. The length of the structural links.
2. The outer diameter with the flexibility of the flexible wheels.
3. The translational stroke of the magnetic sliding mechanism.

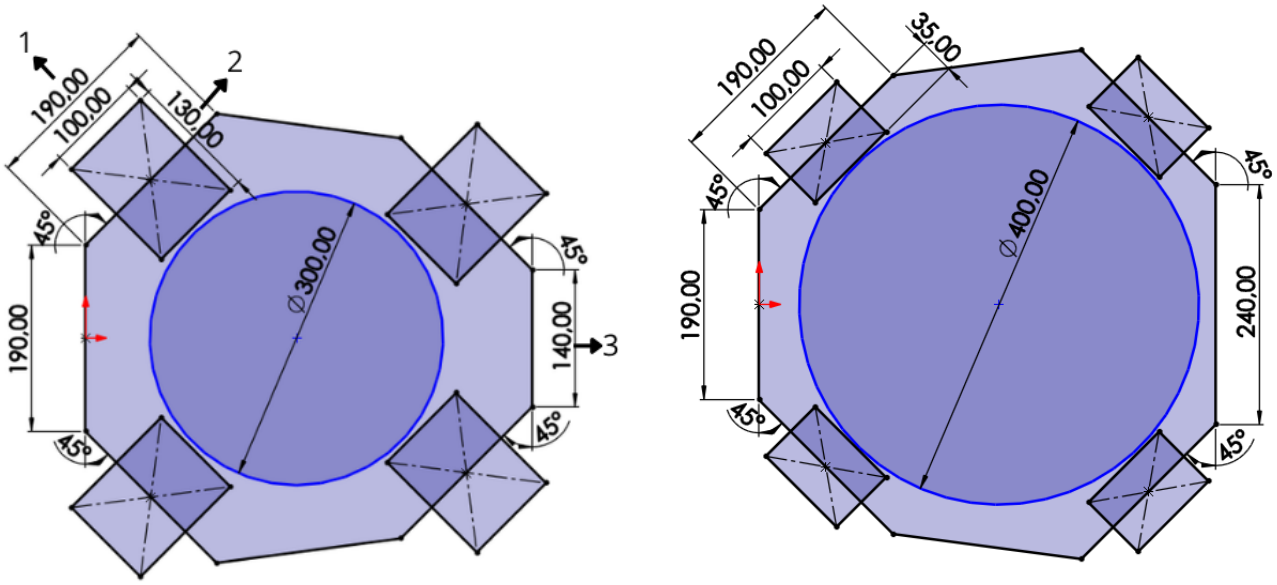

Figure 3.1: Geometric compatibility relies on the relationship between the 190 mm link length, the 130 mm flexible wheels able to indent 30 mm, and the magnetic slider's 140–240 mm translational stroke. This arrangement ensures continuous contact and secure locking for base pipes (300 mm) up to fouled environments (400 mm).

The configuration shown in Figure 3.1 is the result of scaling the components to meet these structural and spatial needs:

- **Wheel Diameter:** A diameter smaller than 130 mm would not provide enough compliance, following from Subsection 4.3 (Figure 4.8). Conversely, a larger wheel would increase the system's weight, inertia, and drag.
- **Link Length:** The 190 mm link size is tied to the wheel diameter. This ratio ensures the gripper maintains contact.
- **Magnetic slider:** The magnetic slider has a specific physical limit: its maximum length is restricted to less than twice its retracted length, minus 40 mm for the magnet housing. Resulting in the magnetic slider moving from 140 mm to 240 mm.

3.2. KINEMATIC COUPLING OF THE WHEELS AND MAGNETIC SLIDER

Having established the static geometric blueprint of the robotic chassis in Section 3.1, it is critical to understand how these spatial constraints govern the system. While the discrete mechanisms, the compliant wheels and the magnetic slider, were evaluated in isolation in Chapter 2, their true operational capability emerges through their mechanical integration. This section details the dynamic synergy between these components, illustrating how the fixed geometric architecture translates localised obstacle impacts into a coordinated, system wide kinematic response.

When a flexible wheel deforms over a marine obstacle, it naturally generates a reactive normal force (F_N). Due to the fixed geometric constraints of the wrapping linkage, a component of this normal force is mechanically transmitted parallel to the sliding rail of the magnetic lock. By summing the relevant force components derived from the Free Body Diagram (Figure 3.2a), the cumulative resultant force (F_{Mx}) acting perpendicular to the sliding rail is mathematically defined by Equation 3.1:

$$F_{Mx} = \sum_{i=1}^{4} F_{N,i} \cos(45^\circ) \tag{3.1}$$

In the current prototype iteration, this transmitted force acts directly on the rigid tendon actuation line. Consequently, manual adjustment of the actuation line via the spool is required to expand the overall circumference of the gripper. This rigid constraint represents a kinematic limitation; to enable the gripper's circumference to momentarily expand and accommodate significantly larger obstacles without disrupting the continuous magnetic locking, intentional compliance should be introduced into the actuation line in future iterations. The necessity of introducing this dynamic compliance to automate expansion is evaluated further in Section 3.5.

3.3. STABILITY

Having detailed the internal kinematic coupling in Section 3.2, it is necessary to evaluate how the stability of the CRAB. While continuous active mobility and payload integration were deliberately isolated from this specific prototyping phase, macroscopic stability remains a fundamental architectural requirement. To ensure that future iterations can successfully achieve continuous mobility, the spatial distribution of mass and buoyancy must be analysed.

Following Figure 3.2a, upward movement occurs when net buoyancy exceeds mechanical friction plus gravity, as defined in Equation 3.2 (with gravity (F_g), variable buoyancy (F_B) and rolling friction (F_r)):

$$F_B > F_g + F_r, \quad \text{for movement upwards} \tag{3.2}$$

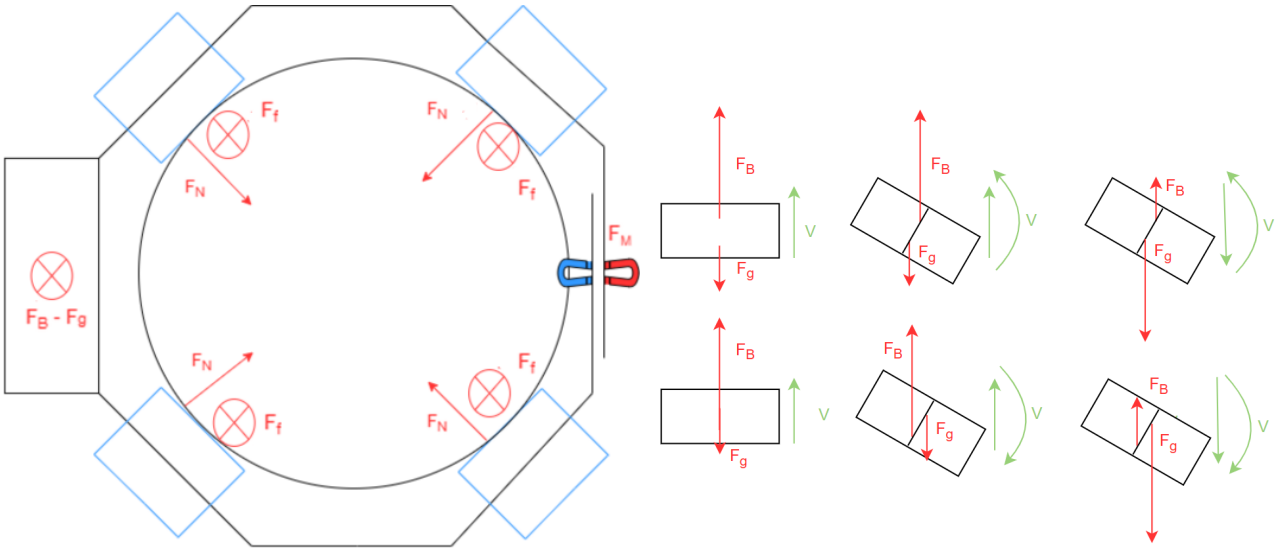

(a) Top-view Free Body Diagram (FBD).

(b) Side-view stability analysis.

Figure 3.2: The FBD (left) defines the vector interactions between gravity (F_g), buoyancy (F_B), magnetic locking (F_M), normal forces (F_N) and rolling friction (F_r) used to derive the mobility equations. The side-view analysis (right) identifies the passive stability requirement: maintaining the centre of buoyancy above the centre of gravity to ensure a restorative moment against external perturbations, for movement upwards and downwards.

The upper row of Figure 3.2b illustrates a hydrostatically stable configuration, wherein the centre of buoyancy (F_B) is positioned above the centre of gravity (F_g). When the device is perturbed from its equilibrium state, this vertical offset generates a restoring moment (indicated by the green vectors) that naturally returns the CRAB to its original orientation. Conversely, the lower row depicts an unstable arrangement where F_B is located below F_g. In this scenario, any angular displacement creates an overturning moment that further destabilises the system. This behaviour is seen for upwards and downwards movement. Consequently, to ensure passive stability during subsea operations, it is critical for future design constraints that F_B maintains strictly above F_g.

3.4. Fabrication Methodology

To empirically validate the theoretical principles established in the preceding sections, the CRAB architecture was translated into a physical prototype. This section details the fabrication methodology and hardware integration required to construct the robotic carrier.

3.4.1. Dimensioning and Materials

As summarised in Table 3.1, the primary structural materials were chosen to balance rapid prototyping feasibility with the mechanical robustness required for the proof of concept. Beyond these core links and flexures, the system's variable circumference locking and actuation rely on the following specific component selections:

- **Magnets:** Passive permanent magnets were selected for the sliding lock. The assembly utilises one primary magnet (Figure A.4) and three secondary magnets (Figure A.5), with technical specifications detailed in the appendix. This strictly mechanical approach deliberately eliminates the architectural overhead and potential failure points associated with active electromagnets.
- **Spool Design:** A custom aluminium spool was turned and milled to manage the high-strength fishing line (Figure A.1). This allows for centralised tension routing to reliably actuate the compliant flexure network and drive tendon system.

Component	Material	Key Dimensions	Justification
Flexures	Spring Steel	1.6 × 10 × 10 mm	High flexibility without plastic deformation; provides a good balance between stability and flexing capability.
Tendon arm segments	PLA CF	Length 190 mm (Sec 3.1), Diameter 15 mm	Strong, readily available 3D printable material suitable for rapid prototyping.
Tendon line	Fishing Line	N/A	Strong, low friction, and highly cost-effective for actuation.

Table 3.1: Overview of material selection and component dimensioning for the primary structure of the CRAB prototype.

3.4.2. Fabrication flexible wheels

The fluid-filled flexible wheels were fabricated in a three-step casting process. First, silicone was poured into separate top and bottom moulds and allowed to fully cure 3.3a. Next, the cured bottom part was filled with water 3.3b. To seal the assembly, a layer of fresh, uncured silicone was applied around the rim of the bottom half to act as an adhesive. The cured top part was then placed directly onto this wet layer B.1. Once this intermediate layer cured, it permanently bonded the two halves together, sealing the water inside and creating a single, continuous wheel.

(a) Mold filled with silicone

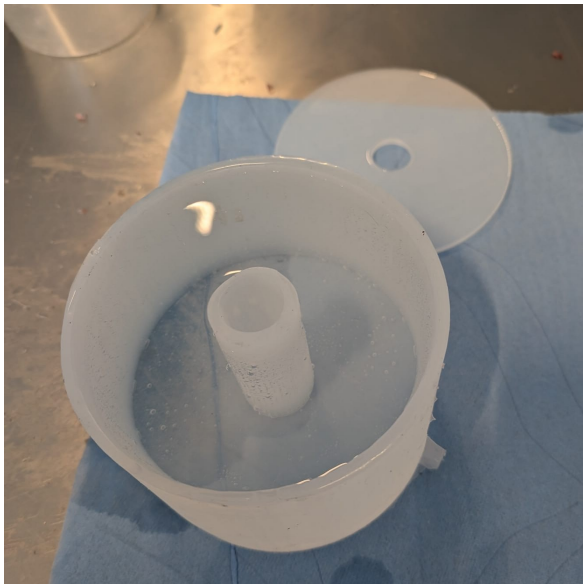

(b) Top part and bottom part with water inside

Figure 3.3: Fabrication process of the flexible wheels

3.4.3. Integration of flexible wheels on the tendon arms

To integrate the flexible wheels with the gripper links, the incorporation of bearings is essential. While ceramic or low absorption plastics are the preferred materials for deep sea bearings to ensure longevity [28], [29], 3D printed PLA bearings was selected for this prototype due to the ease of integration.

Although these components are expected to degrade faster, and have more friction, than their industrial counterparts, they are sufficient for validating the "proof of concept". The assembly consists of metal ball bearings secured within a 3D printed cage; both the central shaft and the outer housing feature 3D printed grooves with a radius matching the balls to ensure relative smooth rotation (Figure A.2 and A.3).

The complete mechanical assembly of the proposed robotic carrier is presented in Figures 3.4, 3.5 and 3.6. These visual representations highlight the physical realisation of the theoretical models, showcasing the direct integration between the primary functional modules. Figure 3.4 illustrates CRAB in a fully open position, while Figure 3.5 and 3.6 detail the variable circumference locking mechanism.

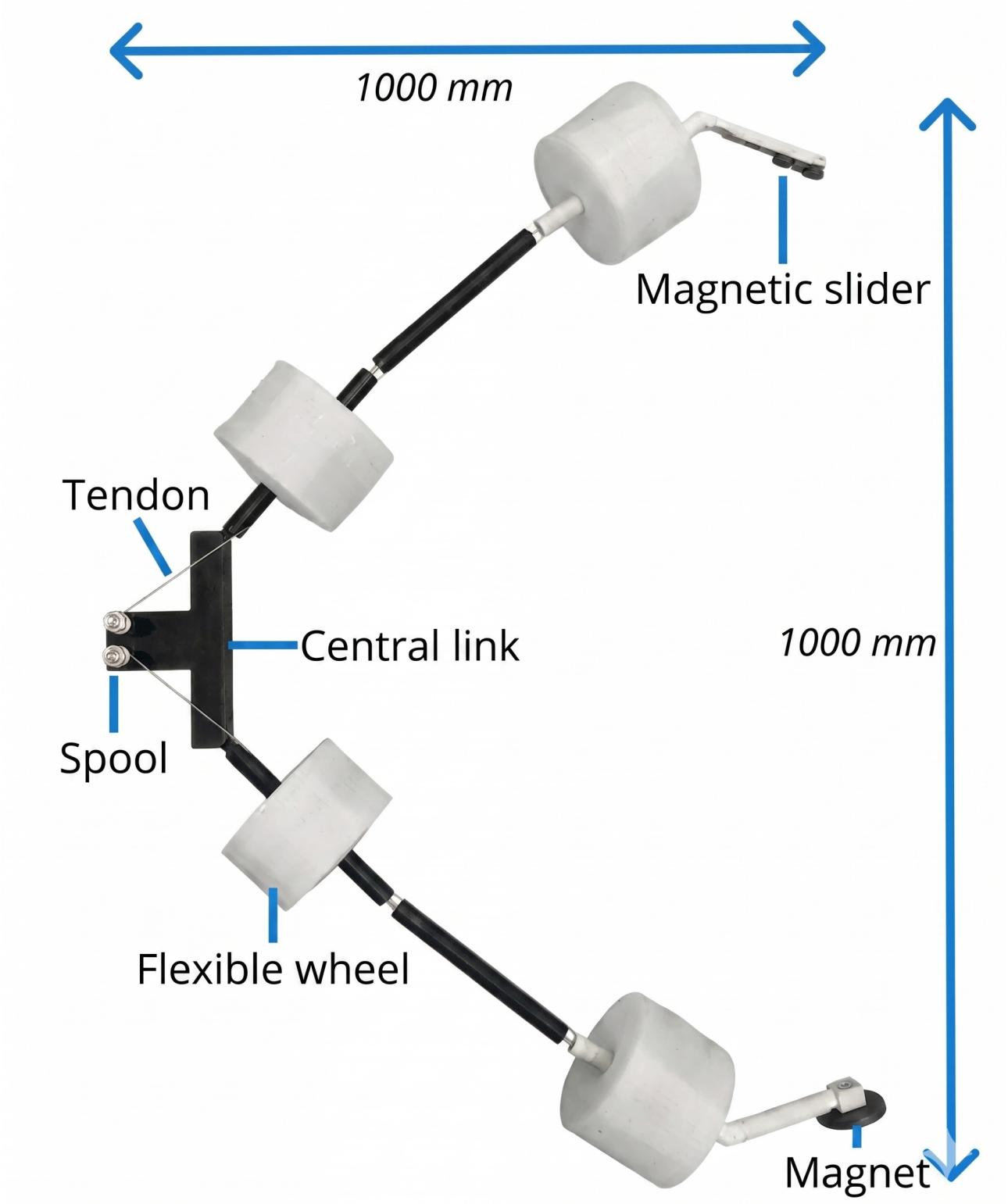

Figure 3.4: Physical realization of the CRAB assembly (1000x1000 mm). This open configuration shows the successful integration of the three-link gripper, the centralized tendon spools, and the four fluid-filled flexible wheels.

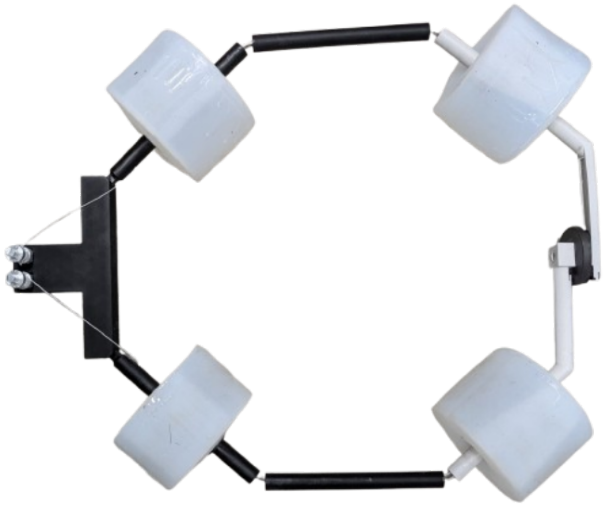

Figure 3.5: Integrated CRAB prototype (500x600 mm) in a closed state. This configuration illustrates the mechanical synergy between the tendon arms and the magnetic slider, demonstrating that the system can maintain a magnetically coupled enclosure.

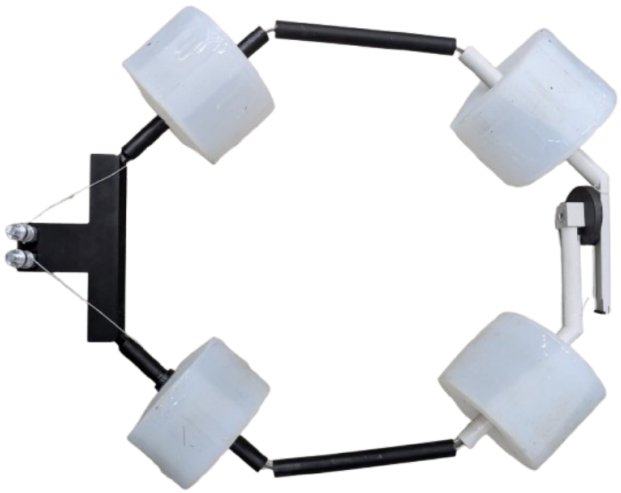

Figure 3.6: CRAB prototype with magnetic slider at its maximum travel. This fully closed configuration demonstrates how the system accommodates varying structural circumference; the sliding mechanism allows the gripper to tighten its hold without decoupling the magnetic lock.

3.5. Discussion

The primary objective of this chapter was to synthesise the isolated mechanisms validated in Chapter 2 into a unified robotic device. To directly address the sub-question regarding how these discrete subsystems can be physically integrated to function as the CRAB prototype, this research concludes that successful integration relies on two core architectural principles: strict geometric compatibility and dynamic kinematic coupling.

First, achieving geometric compatibility required establishing a precise spatial equilibrium between the structural links, the 130 mm diameter of the flexible wheels, and the variable stroke of the magnetic slider. This static spatial arrangement ensures the system can theoretically scale to enclose the 300 mm to 400 mm target diameters. Second, the architecture relies on a magnetic slider for variable circumference locking. When the wheels deform over the obstacles, reactive normal forces will be mechanically transmitted to the magnetic lock. By integrating a passive structural spring in future designs, this coupling would allow the slider to momentarily expand the enclosure to clear the obstacle and then contract after passing the obstacle, without active control.

While the physical assembly successfully validates the spatial and structural feasibility of the CRAB concept, evaluating the static prototype immediately revealed several inherent mechanical limitations. During integration, it was observed that the 3D-printed bearings exhibit inconsistent rotational friction due to natural manufacturing variations. Furthermore, the unconstrained nature of the magnetic slider along its linear rail introduces a clear risk of lateral misalignment post-actuation. To ensure the slider reliably returns to its baseline position for consistent re-engagement, future iterations can integrate a restorative mechanism, such as a low-force passive spring. Which guides the magnetic slider back whenever it's not engaged.

Furthermore, the physical realisation of the prototypes highlighted critical material and fabrication constraints. The Dragon Skin 30 silicone was selected for rapid prototyping; while it successfully demonstrated passive deformation, it lacks long-term abrasion resistance. Future iterations should transition to industrial-grade marine rubbers or specialised polyurethane blends. Beyond offering superior structural durability, polyurethanes possess a significantly lower coefficient of friction compared to silicone. This

characteristic is highly beneficial for subsea mobility, as it would minimise rolling resistance and reduce the likelihood of the flexible wheel to snagging or tearing on sharp biofouling. Furthermore, the multi-part moulding process created structurally weak seams. Redesigning the fabrication methodology to cast the wheel as a single, continuous piece would eliminate these weak points and reduce manufacturing variables.

Ultimately, while this chapter demonstrates that the discrete subsystems can be successfully integrated into a cohesive physical proof-of-concept, the theoretical kinematic relationships and structural tolerances discussed here cannot be fully validated through static assembly alone. To quantify the system's actual operational capabilities, observe dynamic coupling in motion, and identify true physical failure thresholds, the integrated prototype must be subjected to empirical testing, which is the focus of Chapter 5.

4. Finite element model of the flexible wheel

While Chapters 2 and 3 established the architectural integration of the flexible wheel, optimising its specific morphological behaviour requires dedicated analysis. Building upon the initial prototyping phase, this chapter isolates the flexible wheels and further investigates their deformation mechanics through Finite Element Analysis (FEA). The chapter is structured as follows: Section 4.1 outlines the operational limitations of existing compliant tyre technologies. Section 4.2 details the computational modelling, empirical calibration of the FEA framework and the simulation parameters used to test various dimensional configurations. Section 4.3 presents the quantitative results, analysing the wheel's structural forces and dynamic kinematic responses. Finally, Section 4.4 synthesises these findings, discussing current limitations and providing actionable recommendations for future material selection and morphological optimisation.

4.1. Background

A critical mechanical challenge in subsea infrastructure inspection is the continuous traversal of irregular biological protrusions. Conventional wheels are engineered for strict load-bearing; consequently, encountering obstacles forces the vehicle to abruptly lift its entire chassis over the geometry. This paradigm differs fundamentally from the proposed flexible wheels, which operate solely as passive kinematic elements designed to deform dynamically around obstructions.

Literature regarding flexible wheel architectures is primarily restricted to terrestrial applications, such as the Tweel [30] and low-pressure balloon tyres [31]. While the Tweel's non-pneumatic, poly-resin spokes offer excellent impact absorption on land, its discrete spoke structure concentrates the vehicle's weight into specific point loads, leading to slipping and debris entrapment when navigating the sharp irregularities of marine growth. Conversely, highly compliant balloon tires are inherently disqualified by their pneumatic nature; the extreme hydrostatic pressures of the deep sea would violently compress their internal volume, completely eliminating their flexibility. To overcome these environmental limitations, this research proposes an enclosed, fluid-filled wheel architecture. By utilising an incompressible internal medium, this design inherently resists hydrostatic compression while uniformly distributing forces across the entire contact patch, allowing the wheel to smoothly envelop subsea obstacles without kinematic stalling.

While the theoretical advantages of a fluid-filled elastomeric wheel are clear, predicting its exact kinematic behaviour presents a significant engineering challenge. The structural interaction between a hyperelastic membrane and an incompressible fluid yields highly non-linear deformation mechanics that cannot be accurately captured through simple analytical equations. Consequently, to optimise the wheel's morphological dimensions, specifically its width, diameter, and membrane thickness, without relying exclusively on trial-and-error physical prototyping, a robust computational framework is required. Therefore, this chapter utilises FEA to isolate and quantitatively evaluate the complex structural forces and dynamic deformation behaviours of the proposed wheel architecture.

4.2. Methodology

To systematically investigate the structural deformation and kinematic behaviour of the flexible wheel, this section outlines the computational and experimental methodologies employed.

4.2.1. Finite element model setup

To evaluate the system's structural behaviour, a finite element model was created utilising Abaqus. The baseline flexible wheel was modelled with a 130 mm outer diameter, a 100 mm transverse width, a 4 mm wall thickness, and 5 mm edge fillets. The hyperelastic silicone was defined using a Mooney-Rivlin strain energy potential, assigning a material density of 1.1×10^{-9} tonnes/mm³. To accurately simulate incompressible volumetric displacement, the internal water volume was modelled as a hydrostatic fluid cavity with a density of 1.0×10^{-9} tonnes/mm³ and a fluid bulk modulus of 2200 MPa.

To replicate the physical kinematics of obstacle traversal, the contact surface was defined as a discrete rigid body subject to an encastre (fully fixed) boundary condition. Mobility was simulated by driving the wheel with a prescribed translational velocity ($v_x = 188.4$ mm/s) and an angular velocity ($\omega_z = -2.898$ rad/s, for the 130 mm baseline, scaled accordingly for alternative diameters), while all remaining degrees of freedom were constrained. Finally, to prevent volumetric locking and ensure numerical stability during severe hyperelastic deformation, the wheel geometry was discretised using a free mesh of C3D10M elements (10-node modified quadratic tetrahedrons) with a global element seed size of 6 mm.

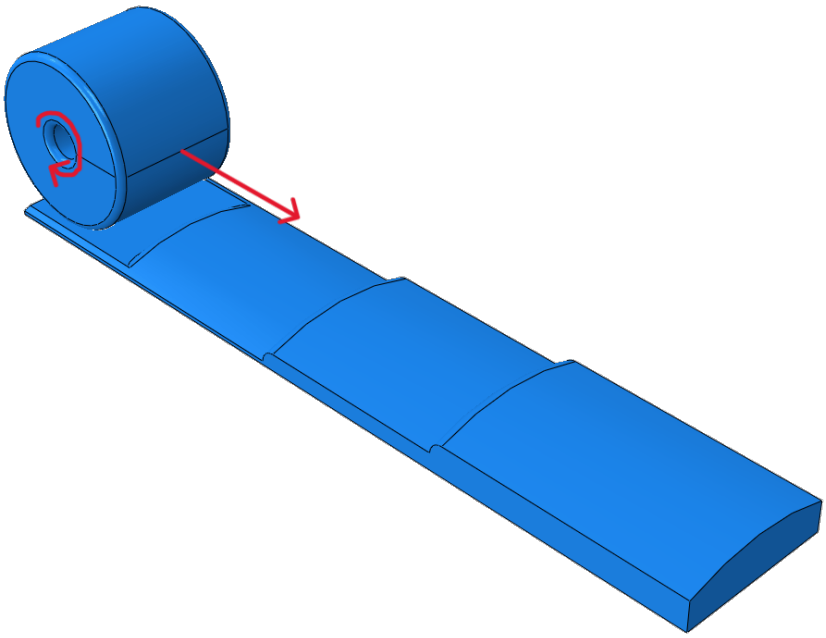

Figure 4.1: FEA simulation environment 130x100 mm wheel. This model utilises sequential 10 mm step increments to evaluate passive compliance during traversal, with the red arrow indicating the simulated direction of motion.

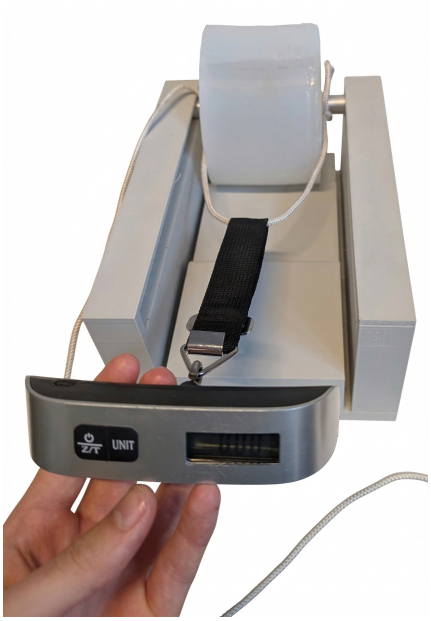

Figure 4.2: Friction measurement setup used for empirical model calibration.

4.2.2. Empirical calibration

To ensure the computational model accurately captures the real-world mechanics of the flexible wheel, the FEA parameters were empirically calibrated. A bench-top experimental apparatus was constructed to physically quantify the requisite boundary forces, explicitly isolating both the structural stiffness and the dynamic rolling friction of the prototype.

Through a series of controlled force-displacement tests (Figures 4.2 and C.1a), the macroscopic, non-linear deformation behaviour of the wheel was systematically measured. The resulting empirical data sets (Figure C.2) served as the quantitative baseline for calibrating the simulation.

Subsequently, an iterative parameter identification process was employed within Abaqus to align the simulated force-displacement response with the physical measurements (Figure C.3). By tuning the material constants to match the empirical values, the optimal material and contact properties for the constitutive model were identified. This calibration yielded the strongest correlation with the physical prototype using the following parameters:

- Hyperelastic constant C_{10}: 0.3
- Hyperelastic constant C_{01}: 0.04
- Material incompressibility parameter D_1: 0.1
- Coulomb friction coefficient: 0.8

To evaluate the mechanical behaviour of the flexible wheel, targeted computational simulations were conducted by altering specific parameters. The wheel's performance was systematically evaluated by independently varying three key dimensions. First, the structural thickness was tested at 2 mm, 4 mm, and 6 mm. Next, the outer diameter was evaluated at 100 mm, 130 mm, and 160 mm (Figure 4.3). Finally, the transverse width was tested at 50 mm, 75 mm, and 100 mm (Figure 4.4). Crucially, to accurately isolate and compare how these dimensional configurations impact obstacle handling, all variations were tested on the exact same simulated surface: a fixed topography featuring sequential step perturbations that progressively increased in height from a baseline of 0 mm up to a maximum of 30 mm in 10 mm increments.

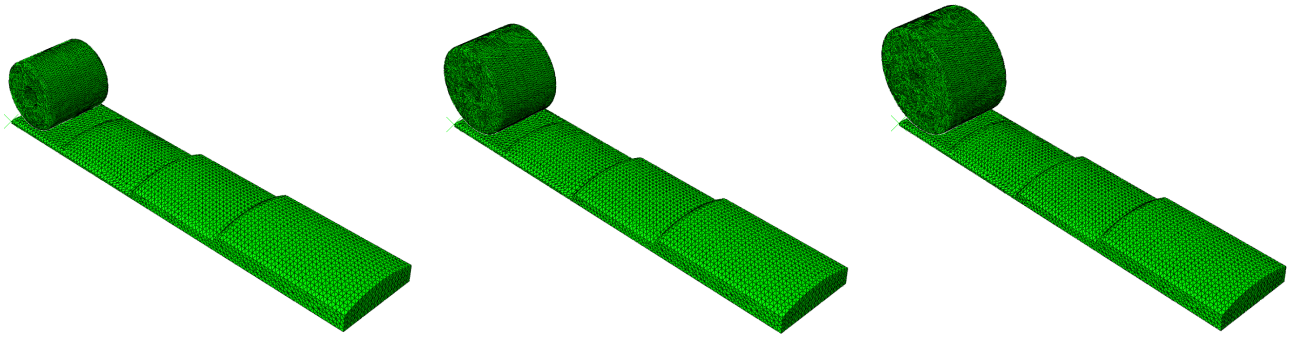

(a) Diameter 100 (b) Diameter 130 (c) Diameter 160

Figure 4.3: Comparison of wheel mesh models with varying outer diameters. The simulation evaluates performance at (a) 100 mm, (b) 130 mm, and (c) 160 mm.

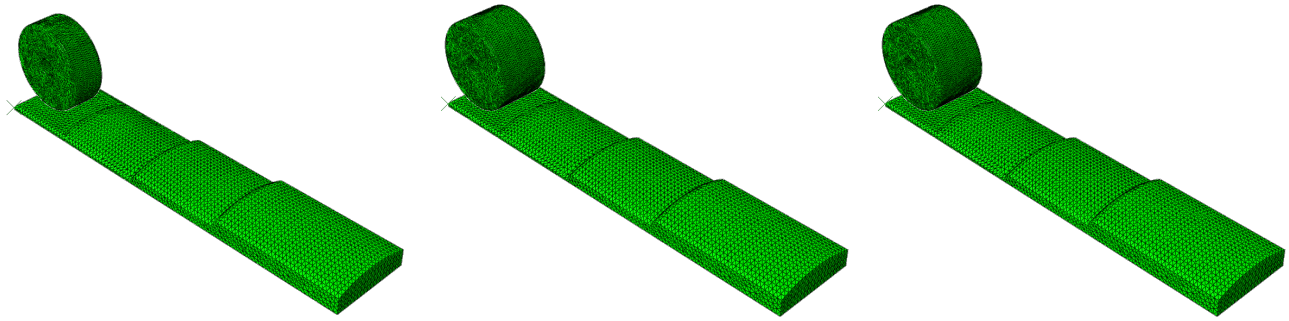

(a) Width 50 (b) Width 75 (c) Width 100

Figure 4.4: Comparison of wheel mesh models with varying transverse widths. The simulation evaluates performance at (a) 50 mm, (b) 75 mm, and (c) 100 mm.

To evaluate the wheel's stability on an off-center surface, an additional simulation tested its behavior under two conditions. First, lateral movement was locked to measure the resulting structural forces; then, this constraint was removed to observe how the wheel naturally tracks and centers itself.

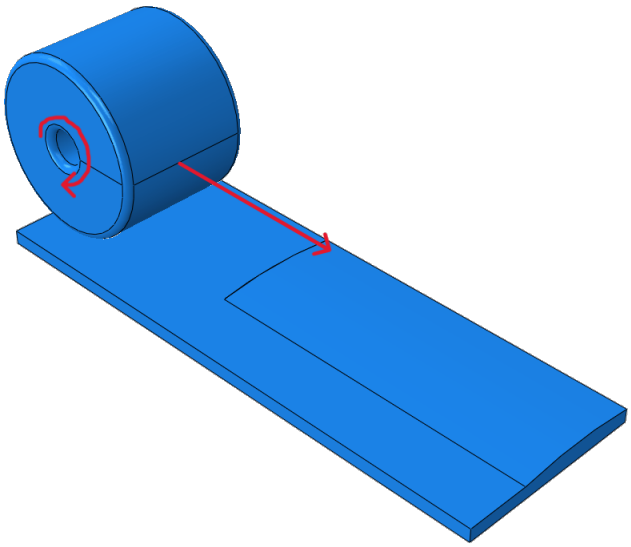

Figure 4.5: Finite Element Analysis (FEA) setup for evaluating kinematic stability. This simulation models the flexible wheel traversing an uncentered obstacle (150 mm radius, 20 mm offset, 4 mm protrusion).

4.3. Results

This section presents the quantitative outcomes of the FEA simulations. To determine the optimal morphology, the structural resistance and dynamic kinematic response of the flexible wheel were evaluated across three varying dimensions: transverse width, membrane thickness, and overall diameter.

First, to evaluate the impact of transverse width, Figure 4.6 illustrates the time-series profiles of the structural forces acting on the flexible wheels during the simulated obstacle traversal, comparing three different transverse widths (50, 75, and 100 mm). Figure 4.6a plots the reactive normal force acting along the vertical axis, while Figure 4.6b captures the corresponding rolling frictional force acting along the axis of travel. As depicted across these configurations, there is an inverse directional correlation between these two metrics: the dynamic fluctuations in the frictional drag exhibit a negative mirroring effect, closely reflecting the shifting magnitudes of the normal force in the negative magnitude throughout the timeline. Furthermore, the simulation data reveal that both forces scale proportionally with the dimension of the wheel. The narrowest wheel (Width 50) exhibits the lowest structural resistance, generating a peak normal force of approximately 15 N and a minimal corresponding frictional drag. Conversely, as the width increases to 75 and 100, the peak normal forces rise significantly to roughly 30 N and 45 N, respectively, resulting in a proportionately larger frictional force exerted on the wider wheels.

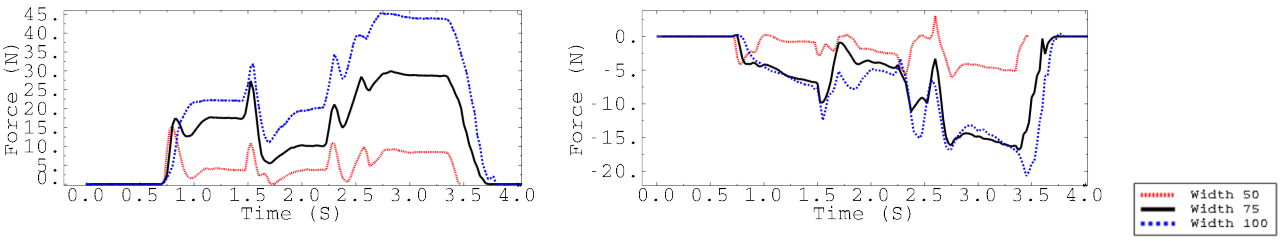

(a) Normal Force (N)

(b) Frictional Force (N)

Figure 4.6: Simulated structural force profiles for flexible wheels of varying transverse widths, showing (a) the reactive normal force and (b) the rolling frictional force. The data indicates that force magnitudes scale proportionally with wheel width.

Then, Figure 4.7 illustrates the effect of wheel thickness on the resulting force over time. The primary trend clearly shows that increasing the thickness of the wheels leads to significantly higher overall and peak

forces. Furthermore, while the absolute force values differ, the force-time behaviour for the wheels with thicknesses of 4 and 6 is remarkably similar, with both displaying comparable plateaus and peak patterns. In contrast, the thinnest wheel (thickness 2) exhibits a noticeably different, more gradual response profile throughout the simulation compared to the thicker models.

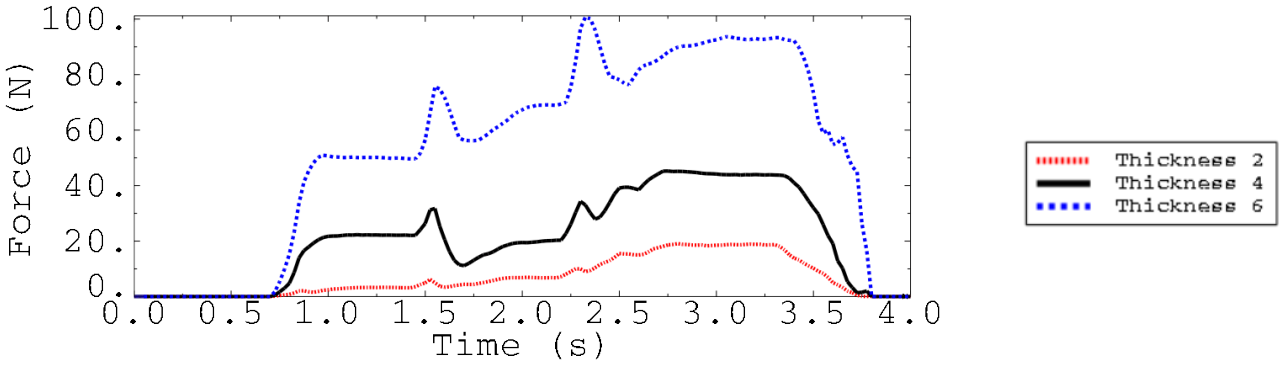

Figure 4.7: Simulated structural force profiles for flexible wheels of varying layer thickness. Increasing thickness from 2 mm to 4 mm and 6 mm results in significantly higher forces.

The graph (Figure 4.8) illustrates a clear inverse relationship between the wheel's diameter and the peak forces experienced during obstacle traversal. The smallest wheel (Diameter 100) exhibits an extreme force spike exceeding 200 N later in the simulation. In stark contrast, as the diameter increases to 130 and 160, the overall force profiles become significantly smoother and lower in magnitude, with peak forces dropping drastically to approximately 45 and 25 N, respectively.

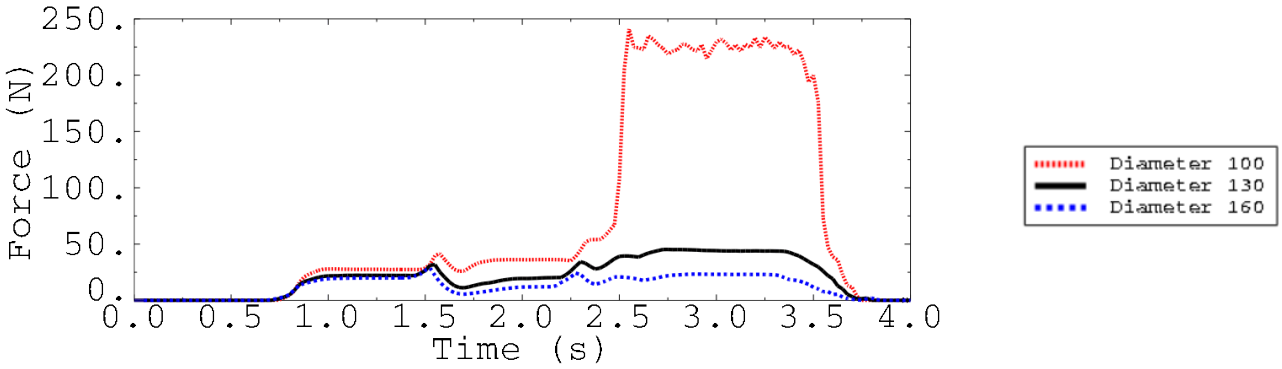

Figure 4.8: Simulated lateral response during off-centre obstacle interaction. The data illustrates (a) the corresponding lateral displacement (U_3) when allowed to move freely and (b) the induced lateral force under locked conditions. The results shows that off-centre impacts generate a restorative forces to automatically centre the system's alignment.

Having established the structural forces during linear traversal, the final simulations evaluated the dynamic kinematic response of the system, further simulations modelled the wheel rolling over an uncentered cylindrical substrate to analyse the lateral stability. The simulated lateral displacement data demonstrates that the flexible wheels passively stabilise, naturally correcting their trajectory to remain centred on the underlying structure (Figure 4.9a). Additionally, these simulations successfully quantified the magnitude of the transverse restorative force responsible for driving the wheel back toward this central mechanical equilibrium (Figure 4.9b).

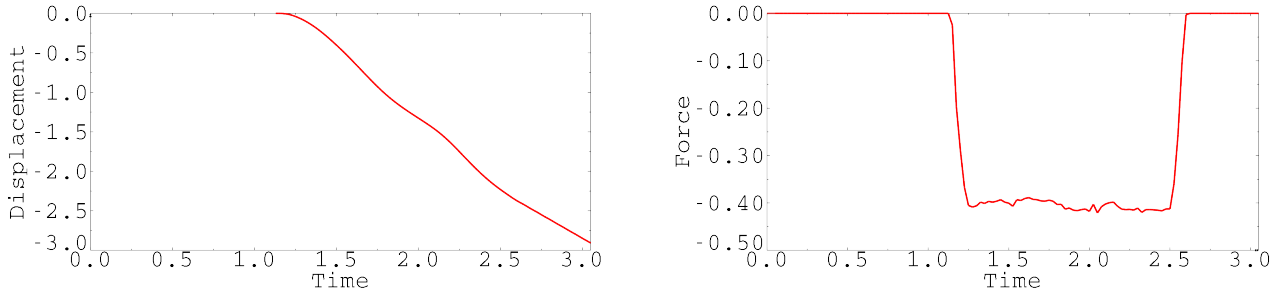

(a) Displacement (mm)

(b) Lateral Normal Force (N)

Figure 4.9: (a) Lateral normal force with lateral movement locked and (b) lateral displacement ($U3$) with lateral movement unlocked for the off-centre test setup.

4.4. Discussion

The primary objective of this chapter was to isolate the fluid-filled flexible wheel architecture and computationally evaluate its non-linear deformation mechanics. To directly address the sub-question regarding how geometric dimensioning affects structural behaviour and stability during obstacle traversal, this research concludes that the wheel's kinematic performance is significantly influenced by a balance between its width, thickness, and overall diameter, while its internal dynamics lead to auto recovery.

While exploring the geometric proportions, the simulation data revealed a direct, proportional relationship between the width of the wheel and the resulting structural forces. The wider wheel configurations generated significantly higher reactive normal forces and frictional drag compared to narrower models. This behaviour can be attributed to the larger contact patch and the increased mass of the internal fluid volume, which together generate higher structural resistance.

Similarly, increasing the membrane's thickness from 2 mm to 4 mm and 6 mm increases this structural stiffness. A thicker hyperelastic wall inherently requires more mechanical work to stretch, resisting initial deformation so that the thicker wheels temporarily act as semi-rigid bodies upon impact, generating severe force spikes before the bulk material finally yields. In contrast, the highly compliant 2 mm membrane yields easily upon impact, smoothly conforming to the obstacle to produce a gradual, dampened force profile.

Just as membrane thickness determines localised stiffness, the overall diameter also dictates the wheel's ability to passively deform. The simulation data points to two practical reasons for the inverse relationship between wheel diameter and peak force. First, larger wheels (e.g., 160 mm) benefit from both their geometry and their internal volume. A larger diameter engages fixed-height obstacles at a shallower approach angle, which reduces sudden impacts. Simultaneously, the larger internal fluid volume easily accommodates the obstacle's shape without causing severe pressure spikes inside the wheel. Second, this behaviour changes completely when the wheel is too small for the obstacle, as seen with the 100 mm configuration. The extreme force spike generated by this smallest wheel is not just the result of a steeper approach angle; it likely indicates that the wheel has simply run out of room to compress. The 100 mm wheel lacks the internal cavity volume to fully absorb the protrusion, forcing the membrane to deform inward until it "bottoms out" against the rigid central hub. At this point of maximum compression, the wheel loses all compliance and effectively acts as a rigid body, causing the severe force spike.

Beyond morphological simulations, stability simulations of the highly compliant wheels revealed a passive auto-centring capability when navigating uncentred obstacles. It is hypothesised that this auto-recovery is fundamentally driven by internal membrane mechanics. When the wheel encounters an off-centre obstruction, the elastomeric exterior undergoes asymmetrical deformation, generating a significant internal tensile stress, or "membrane force," as the continuous material resists the localised strain. As this tensile force pulls inward to return the wheel to its lowest energy state, it resolves into a net transverse restorative force. Consequently, the wheel is passively pulled inward, automatically correcting its trajectory to maintain central alignment over the geometry without the need for active steering.

Furthermore, it is critical to acknowledge that the empirical data used to calibrate the finite element

model inherently contains physical deviations from the idealised computational setup. While the Abaqus simulation strictly isolates the hyperelastic deformation and rolling friction of the wheel, the physical bench-top calibration apparatus introduced several unmodeled forces. Specifically, the measured force-displacement results absorbed additional mechanical resistance from the friction of the bearings, the tension of the actuation rope, and the sliding of the central shaft along its track. Because these systemic frictional forces were present in the physical trial but absent in the digital environment, the resulting calibrated material parameters (such as the hyperelastic constants) likely overcompensate slightly to account for the test rig's mechanical resistance. Consequently, while the calibrated model provides a functional baseline, it does not perfectly isolate the pure material mechanics of the flexible wheel itself.

Finally, while morphological optimisation was not explored in this phase, future iterations should transition the flexible wheel from its current flat-sided profile to a concave, U-shaped cross-section featuring outward-curving, filleted sidewalls. This geometric shift primarily addresses two critical mechanical factors: stress distribution and macroscopic stability. First, flat sided designs contain sharp, 90 degree corners that act as stress concentrators. Replacing these with curved, filleted sidewalls eliminates these vulnerable weak points. By smoothing the geometry, these rounded transitions more evenly distribute volumetric compressive and tensile stresses across the entire membrane during obstacle impacts, mitigating sharp localised strains and significantly enhancing the wheel's operational longevity. Second, a U-shaped geometry naturally nests against the convex subsea pipe, functioning much like a saddle, which will increase the stability.

5. Case study/lessons learned

Following the subsystem evaluation, integration and computational modeling established in preceding chapters, this chapter presents a case study to empirically validate the physical performance of the integrated CRAB prototype. To systematically assess the robotic carrier's operational viability, a series of tests were designed to test its performance against the behavioural requirements. Section 5.1 details the experimental setup utilised to isolate and evaluate the system's core kinematics, specifically focusing on gripping, variable circumference locking and obstacle handling. Section 5.2 presents the observable results and mechanical outcomes derived from these trials. Finally, Section 5.3 provides a critical discussion of these findings, analysing the prototype's traversal successes, structural limitations, and the underlying kinematic causes of any observed mechanical failures.

5.1. Experimental setup

To systematically evaluate the mechanical viability and kinematic performance of the integrated CRAB prototype, a series of controlled empirical trials was conducted. The experimental setup was explicitly designed to isolate and observe the system's response to the core behavioural requirements.

5.1.1. Gripping

To empirically validate the system's geometric compliance and adaptive grasping capabilities, an enclosure test was performed, which is schematically shown in Figure 5.1. The CRAB prototype was positioned on a flat surface with and without a pipe (pipe with 300 mm diameter); tension was incrementally applied to the primary actuation tendon. To generate the necessary winding torque on the central aluminium spool, a motorised drill was utilised. This controlled actuation isolates the kinematic trajectory of the underactuated flexure arms, evaluating their ability to achieve a continuous enclosure and successfully engage the magnetic lock. Validating this wrapping motion is critical, as it demonstrates that the inherent material compliance of the tendon-driven architecture can achieve a locked state without requiring complex, multi-joint active control.

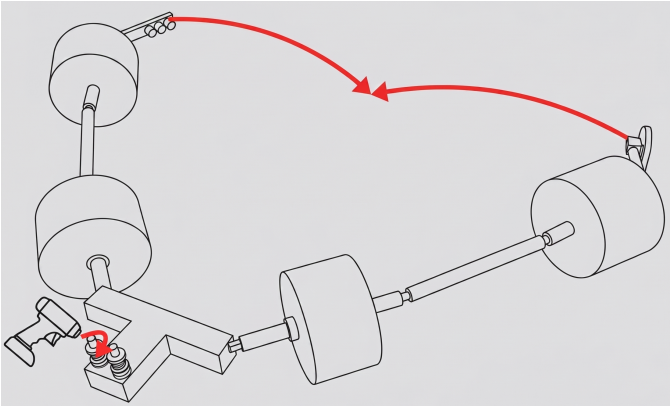

Figure 5.1: Schematic of the empirical test setup used to validate the tendon-driven gripping kinematics. The schematic defines the controlled, drill-actuated trajectory used to physically verify the enclosure capabilities of the tendon arms.

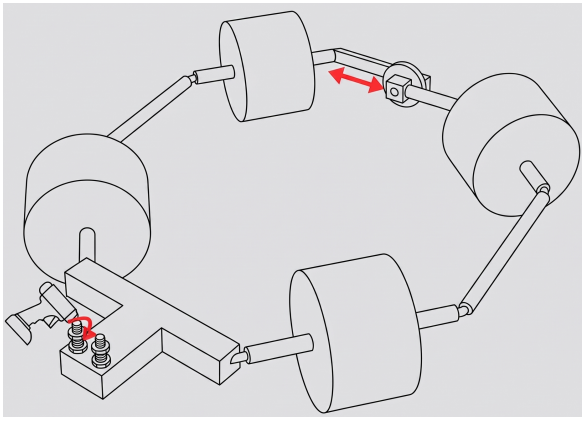

Figure 5.2: Schematic of the empirical test setup used to evaluate the variable circumference lock. This setup illustrates how drill actuation is applied to evaluate whether the CRAB can tighten its grip without decoupling.

5.1.2. Variable circumference locking

To empirically evaluate the efficacy and structural robustness of the variable circumference locking mechanism, a controlled test was conducted, which is schematically shown in Figure 5.2. Initially, the CRAB prototype is brought into a fully closed and magnetically engaged position. Subsequently, continuous tension is applied to the tendon line utilising the same motorised actuation method established during the gripping test to further reduce the system's circumference while maintaining the locked state.

This experimental setup actively forces the magnetic slider to translate along its rail under actuation. Evaluating the system's response to this actuation will verify whether the inherent compliance of the architecture allows the robotic device to accommodate varying structural diameters.

5.1.3. Obstacle handling

A controlled test was conducted to empirically validate the system's passive obstacle-handling capabilities, as illustrated in Figure 5.3. During the test, the CRAB prototype was manually translated along the longitudinal axis of a 300 mm diameter cylindrical pipe. To simulate different severities of subsea biofouling, this test structure was fitted with rigid, discrete radial protrusions with radius of 30 mm, 40 mm, 50 mm, and 60 mm (Figure 5.4). Guiding the device over these geometries facilitated direct observation of wheel deformation and, working in tandem with the magnetic slider, demonstrated the CRAB prototype's obstacle handling capabilities.

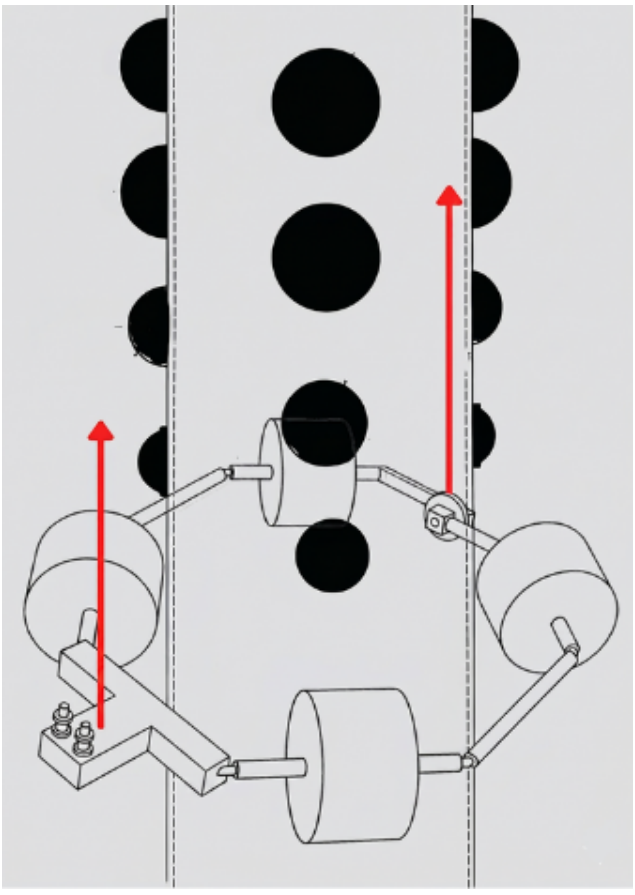

Figure 5.3: Schematic representation of the CRAB prototype moving along the cylindrical test setup, with its movement path indicated by red arrows.

Figure 5.4: Experimental setup for obstacle handling, featuring a 0.3 m diameter pipe with rigid protrusions of 30, 40, 50, and 60 mm radius.

5.2. Observations

This section presents the empirical outcomes derived from the physical tests. The findings are systematically categorised to reflect the CRAB prototype's performance across its behavioural requirements: gripping (Section 5.2.1), variable circumference locking (Section 5.2.2) and obstacle handling (Section 5.2.3). The objective of this section is to report the observable mechanical behaviours, kinematic responses, and physical failure thresholds encountered during testing. An analysis of these outcomes, including the underlying causes of mechanical failures and subsequent design implications, is deferred to the Section lesson learned 5.3.

5.2.1. Gripping

During the enclosure test, the actuation of the CRAB prototype was successful (Figure 5.5), showcasing the ability to enclose diameters of 300 mm in diameter. Following the application of tension to the primary tendon, the underactuated flexure arms executed an enclosing trajectory. This kinematic motion demonstrated the inherent material compliance of the design, allowing the arms to form the required circular enclosure and successfully align and engage the magnetic lock. Ultimately, these empirical results validate the system's ability to achieve a secure grasp utilising a simple, tendon mechanism without the need for complex active control (see Figure 5.5).

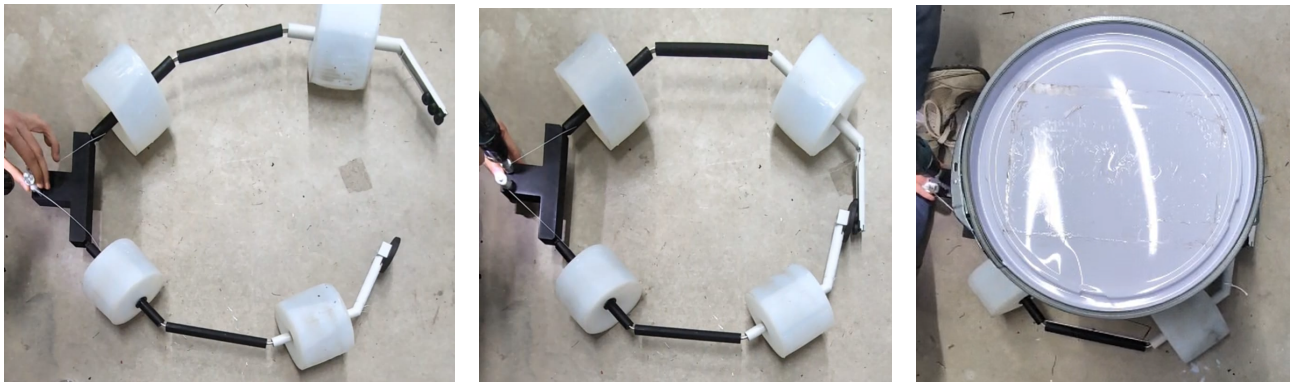

(a) Open CRAB (b) CRAB closed and locked (c) Gripping 300 mm diameter

Figure 5.5: Supplementary visual documentation, in the attached files, of the gripping results. The footage validates the CRAB prototype successfully executing its enclosing trajectory both in free space and around a target pipe.

5.2.2. Variable circumference locking

The empirical evaluation of the variable circumference locking mechanism demonstrated significant limitations (see Figure 5.6). During the dynamic adjustment trial using a motorised drill at half power, the magnetic slider only moved a minimal amount. However, the slider moved easily with negligible resistance when a light force was applied directly parallel to its linear rail, by hand (Figure 5.6b). The results of these tests are analysed further in the Section Lessons Learned 5.3.

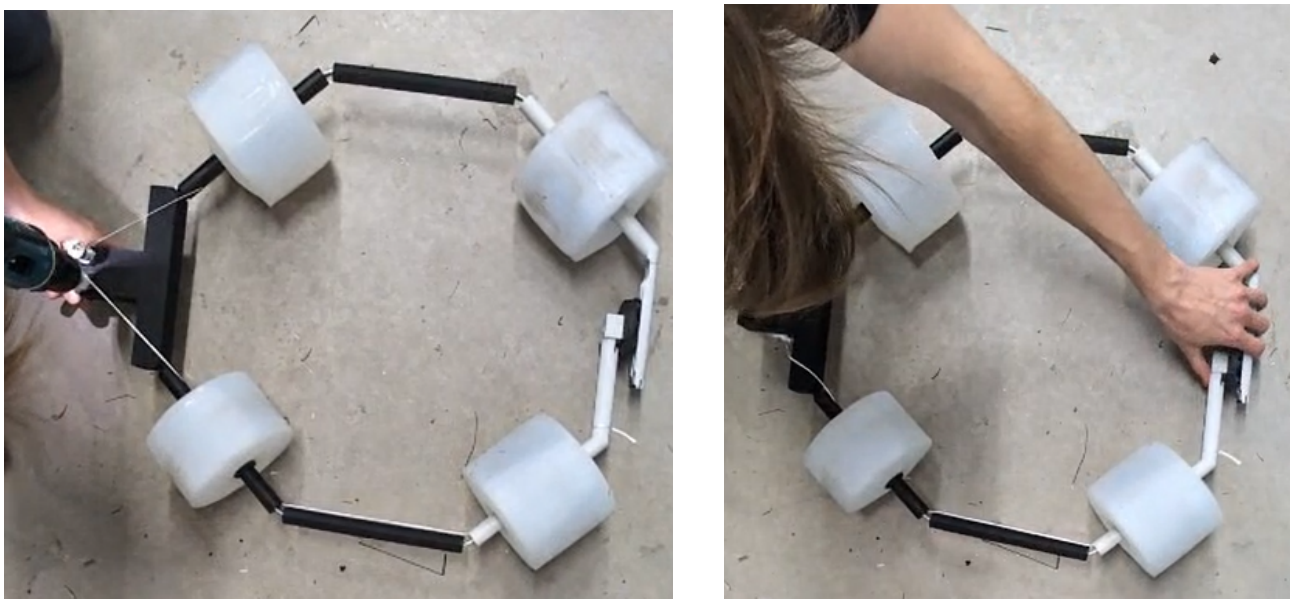

(a) Actuated by drill

(b) Actuated by hand

Figure 5.6: Supplementary visual documentation, in the attached files, showing the variable circumference locking results. The video data captures the system's restricted movement when driven by the central spool, alongside the negligible resistance observed during manual actuation.

5.2.3. Obstacle handling

Empirical testing demonstrated that the CRAB prototype successfully navigated radial obstacles measuring 30 mm, 40 mm, and 50 mm without mechanical stalling. However, the system exceeded its operational threshold during the 60 mm obstacle, resulting in a structural rupture of one of the flexible wheels (see Figure 5.7). This material failure highlights a critical limitation in the current iteration's design, the mechanical causes and implications of which are analysed comprehensively in the Section Lesson Learned 5.3.

(a) Compliance of 50 mm obstacle.

(b) Wheel rupture at 60 mm obstacle.

Figure 5.7: Supplementary visual documentation, in the attached files, showing the obstacle handling result. These recordings verify the CRAB's ability to navigate simulated biofouling (30–50 mm) without mechanical stalling. The footage captures the subsequent structural failure at the 60 mm protrusion.

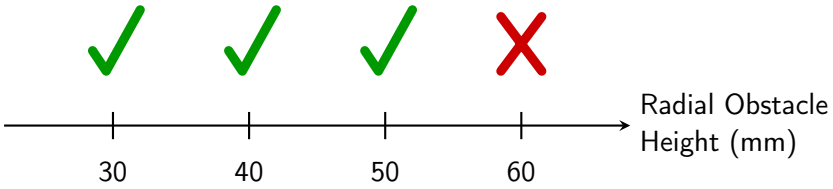

Figure 5.8: CRAB obstacle handling evaluation: Successful traversal up to 50 mm (green checks) followed by failure at 60 mm (red cross).

5.3. Lessons Learned

To directly address the sub-question regarding the system's operational capabilities, the empirical trials successfully validated the prototype's primary operational sequence. By applying incremental tension to the primary actuation tendon, the underactuated flexure arms reliably executed an enclosing trajectory, achieving a stable, enveloping enclosure around a 300 mm diameter pipe. This unhindered wrapping motion demonstrated that the inherent mechanical compliance of the tendon-driven architecture can effectively achieve a secure grasp and facilitate the correct spatial alignment required to engage the magnetic lock, all without the necessity for complex control systems. Crucially, establishing this secure baseline enclosure on the 300 mm pipe allowed the prototype to subsequently satisfy its mobility requirement, successfully navigating simulated radial marine biofouling up to 50 mm in height along that same structure without mechanical stalling.

However, pushing the system beyond this to a 60 mm protrusion exposed a critical physical failure. This obstacle induced a rupture in the flexible wheel, which propagated along a previously identified weak layer 3.4.2. This failure was mechanically exacerbated by the placement of the internal bearing; because the bearing did not completely support the seam, the overhanging material was subjected to acute shear forces. While continuous underlying bearing support would likely prevent this specific rupture, the event highlights the limitations of the current fabrication methodology and reinforces the need to transition to single-piece continuous casting to ensure operational longevity, supporting this suggested improvement in Subsection 3.5.

Furthermore, the empirical evaluation of the variable circumference locking mechanism revealed severe kinematic conflicts. The system experienced significant resistance generated by both the flexible wheels and the sliding magnetic lock. While moving the magnetic slider by hand demonstrated negligible resistance, when actuated by the drill, severe resistance was observed. The spatial trajectory of the grasping motion structurally constrains the sliding element. Instead of translating parallel to the linear rail, the gripper arms impart a angular misalignment. This off-axis load drives the slider against the rail walls, causing it to jam. To resolve this kinematic conflict in future iterations, two primary architectural modifications are proposed: significantly decreasing the width of the sliding element to increase its tolerance for angular misalignment, or fundamentally redesigning the linear track into a accurately calculated curved rail that matches the wrapping trajectory of the gripper arms.

Although empirical validation was strictly restricted to cylindrical test structures, the inherent compliance of the tendon-driven soft gripper suggests the architecture could theoretically accommodate more complex, continuous geometries. Ultimately, these empirical trials successfully validated the CRAB prototype's foundational concept. Moving forward, addressing the critical mechanical thresholds exposed during testing, specifically material rupture and stalling of the magnetic slider, establishes a clear roadmap for the next phase of development.

6. Conclusion

This final chapter synthesises the theoretical analyses, computational modelling, and empirical findings of this research to evaluate the overall viability of the CRAB prototype. The overarching objective of this thesis was to develop an adaptive, continuous-motion underwater device capable of overcoming the geometric irregularities and biological unpredictability inherent in unstructured subsea infrastructure. To address this complex challenge, the research systematically progressed from the morphological evaluation of isolated mechanical subsystems to the physical integration and empirical validation of the CRAB. Section 6.1 directly answers the foundational research questions, presenting the final conclusions drawn from the prototype's successes and physical failure thresholds. Subsequently, Section 6.2 critically examines the material, kinematic, and methodological limitations encountered during this initial proof-of-concept phase. Finally, Section 6.3 outlines targeted recommendations for future work, emphasising the necessary morphological evolutions and structural refinements required to advance the system toward robust, autonomous field deployment.

6.1. Summary of findings

The overarching objective of this research was to develop an adaptive underwater device to overcome the geometric irregularities and biological unpredictability inherent in subsea infrastructure. To address this complex mechanical challenge, the problem was divided into discrete inquiries evaluating subsystem viability, physical integration, morphological optimisation of the flexible wheels, and physical tests.

Regarding the necessary mechanical subsystems, a morphological map and empirical evaluation established that a tendon-driven gripper utilising a three-link, two-flexure configuration successfully balances the required kinematic predictability with the spatial flexibility needed to adaptively enclose subsea pipes. To achieve continuous mobility over irregular marine growth, passive water-filled flexible wheels were identified as the optimal architecture to prevent mechanical stalling. Furthermore, a passive permanent magnetic sliding lock was selected to provide dynamic coupling.

Computational analysis evaluating the morphology of the fluid-filled wheels established a proportional relationship between the wheel's transverse width and both its reactive normal force and frictional drag. Furthermore, it demonstrated that increasing the thickness of the silicone also results in a increase in these normal forces. Conversely, increasing the overall wheel diameter was shown to decrease resistance and improve passive compliance during obstacle handling. Dynamic simulations also confirmed that the fluid-filled wheels possess inherent passive auto-centering capabilities when rolling over uncentered cylindrical surfaces.

Finally, physical trials tested the operational capabilities of the prototype and showcased the proof of concept, demonstrating that the CRAB can successfully achieve a grasp (around a pipe with a 300 mm diameter). Furthermore, the system demonstrated the capacity to navigate radial obstacles up to 50 mm in radius without stalling. However, limitations were shown when a 60 mm obstacle induced a structural rupture in the flexible wheel, and variable circumference locking attempts failed when angular misalignment caused the sliding track to jam.

Ultimately, the physical trials showcased the proof of concept by successfully executing the system's primary operational sequence: the CRAB prototype encloses a 300 mm diameter pipe and navigates simulated radial biofouling up to 50 mm in radius without mechanical stalling. By achieving this mobility, the empirical findings confirm that relying on passive material compliance offers a viable foundational methodology for moving along unstructured subsea infrastructure.

6.2. LIMITATIONS

The findings of this CRAB device are subject to several specific mechanical, material, and methodological limitations:

- *Material fragility:* The selection of Dragon Skin 30 silicone for the compliant membranes, 3D-printed PLA CF for the structural components and the internal bearings was dictated primarily by rapid prototyping constraints. For future development, it is important to recognise that these specific materials are not superior to other available options.
- *Fabrication inconsistencies:* The multi-part moulding process utilised for the flexible wheels created structurally weak seams that proved vulnerable to stress, leading to the wheel rupturing on the 60 mm obstacle. Additionally, manufacturing variations in the 3D-printed bearing components introduced unpredictable and inconsistent rolling friction across the four wheels.
- *Magnetic slider:* The linear magnetic track design proved geometrically incompatible with the non-linear spatial trajectory of the wrapping gripper arms. This discrepancy introduced severe off-axis loading and angular misalignment, causing the slider to jam against the rail walls and substantially increase the system's kinetic friction.
- *Flexible wheel shape and internal material:* The current flat-sided cross-sectional profile of the flexible wheel, and its internal water fluid, are not optimised.
- *Drive mechanism and payload integration:* Drive systems and inspection payloads were intentionally excluded from this prototyping phase to strictly isolate and validate the robot's core behavioural requirements. Because of this, the prototype's macroscopic stability and active mobility in motion remain unverified. Transitioning to a field-ready platform will require substantial structural modifications to accommodate these heavy components.
- *Dynamic stability:* Apart from the deliberate exclusion of a physical continuous drive mechanism, the macroscopic stability of the system in motion remains unverified. Maintaining dynamic equilibrium, specifically preventing the chassis from unpredictable pitching, rolling, or wedging, is paramount. Without stable kinematics during active motion, the system is highly susceptible to mechanical stalling, regardless of the wheels' individual compliance. Therefore, a more in-depth, comprehensive analysis of the system's rolling dynamics and macroscopic stability is required.
- *Infrastructure geometry:* Empirical validation was strictly restricted to continuous, cylindrical test structures. The system was not tested on non-cylindrical or discontinuous surfaces.

In conclusion, while the CRAB prototype successfully demonstrates passive compliance, its operational viability is hindered by critical limitations. The use of rapid-prototyping materials restricts durability and introduces structural inconsistencies. Furthermore, kinematic conflicts within the variable circumference locking mechanism lead to jamming. Finally, the system's dynamic stability remains entirely unverified due to the exclusion of continuous drive systems and payload integration, and its traversal capabilities were solely validated on continuous cylindrical test structures. Acknowledging these material, kinematic, and methodological constraints establishes a clear roadmap for necessary future refinements.

6.3. FUTURE WORK

To advance the CRAB architecture toward robust operational deployment, future research and development must prioritise the following iterative design improvements:

- *Material:* Transitioning from rapid-prototyping silicones to industrial-grade marine rubbers or specialised polyurethane blends is essential for achieving long-term subsea abrasion resistance. Additionally, replacing the 3D-printed PLA CF used for structural components and internal bearings with more robust, long-lasting materials is important for ensuring the system's overall operational longevity.
- *Fabrication improvements:* Redesigning the flexible wheel moulds to facilitate a single-piece, continuous cast will eliminate structural weak points at the seams and significantly reduce manufacturing

variables.

- *Kinematic refinement of the magnetic slider:* To resolve this mechanical jamming, future iterations must either redesign the linear rail into a curved track that aligns with the gripper arms' natural trajectory or significantly reduce the width of the sliding element to increase its tolerance for angular misalignment.
- *Morphological redesign of wheels and internal fluid selection:* To optimise stress distribution and durability, the flat-sided geometry should transition to a concave, U-shaped cross-section with filleted sidewalls. Eliminating sharp 90-degree corners removes critical stress concentrators, distributing deformation forces evenly to prevent material rupture. Furthermore, this U-shape acts as a mechanical saddle; any lateral drift asymmetrically stretches the membrane against the pipe's curve, generating a restorative force that naturally drives passive auto-centring. Additionally, replacing the internal water volume with non-Newtonian shear-thickening fluids (STFs) could provide inherent passive damping against dynamic collisions. Crucially, the efficacy of these structural and fluidic modifications can be evaluated using Abaqus simulations.
- *Payload and drive integration:* Subsequent iterations must integrate reliable, continuous drive systems and a payload. This will require substantial structural modifications to accommodate the increased payload without compromising the established adaptive kinematics.
- *Dynamic stability:* A critical requirement for transitioning the CRAB from a proof-of-concept to a field-ready device is a comprehensive analysis of its macroscopic stability. Future research must evaluate the system's dynamic stability when navigating irregular infrastructure. This investigation should quantify the kinematic limits required to maintain geometric equilibrium and prevent the chassis from pitching, rolling, or mechanically wedging during continuous mobility.
- *Discontinuous infrastructure:* Addressing the complex dynamics of discontinuous infrastructure requires a fundamental reevaluation of the initial morphological assumptions governing the mobility and drive subsystems. While the current single-plane grasping mechanism can be sufficient for continuous cylinders, it inherently lacks the macroscopic stability required to navigate discontinuous infrastructure. A highly promising direction for this morphological evolution is the transition to a spatially distributed, parallel dual-gripper architecture, conceptually similar to the AURI device. By utilising two sets of wheel-equipped gripper arms oriented parallel to one another with a defined spatial separation, this multi-segment configuration would bridge the structural voids between discontinuous infrastructure. This ensures continuous multi-point contact, thereby providing the uninterrupted traction and structural stability necessary for active mobility on highly discontinuous infrastructure.

As global offshore infrastructure expands into deeper, more challenging environments, the demand for adaptable inspection technologies will only intensify. While the current CRAB prototype must still overcome immediate kinematic and material hurdles, solving these challenges lays the groundwork for a fundamental paradigm shift in subsea maintenance. By transitioning away from destructive "clean-and-traverse" crawlers in favour of the Compliant Robotic Architecture for Biofouling (CRAB), future iterations of this system offer great potential. They stand to drastically reduce operational downtime, prevent abrasive damage to vital pipelines, and mitigate environmental disruption, ultimately safeguarding the critical underwater infrastructure that power and connect the modern world.

REFERENCES

[1] Lars Johanning. Load and fatigue evaluation for 66kV floating offshore wind submarine dynamic power cable. January 2019.

[2] Rasul Satymov, Dmitrii Bogdanov, and Christian Breyer. Techno-economics of offshore wind power in global resolution. *Applied Energy*, 393:125980, September 2025.

[3] David Young. Predicting Dynamic Subsea Cable Failure for Floating Offshore Wind.

[4] E. Gulski, G. J. Anders, R. A. Jongen, J. Parciak, J. Siemiński, E. Piesowicz, S. Paszkiewicz, and I. Irska. Discussion of electrical and thermal aspects of offshore wind farms' power cables reliability. *Renewable and Sustainable Energy Reviews*, 151:111580, November 2021.

[5] Why Europe needs a Strategic Roadmap for Submarine Cable Resilience, October 2025.

[6] Simona Aracri, Francesco Giorgio-Serchi, Giuseppe Suaria, Mohammed E. Sayed, Markus P. Nemitz, Stephen Mahon, and Adam A. Stokes. Soft Robots for Ocean Exploration and Offshore Operations: A Perspective. *Soft Robotics*, 8(6):625–639, December 2021.

[7] Undersea Hybrid Threats in Strategic Competition: The Emerging Domain of NATO–EU Defense Cooperation.

[8] Wenshuo Tang, Keith Brown, David Flynn, and Hugues Pellae. Integrity Analysis Inspection and Lifecycle Prediction of Subsea Power Cables. In *2018 Prognostics and System Health Management Conference (PHM-Chongqing)*, pages 105–114, Chongqing, October 2018. IEEE.

[9] Central Mechanical Engineering Research Institute, Durgapur 713209, India, P. Chattopadhyay, S. Ghoshal, Department of Mechanical Engineering, Indian Institute of Technology(ISM), Dhanbad 826004, India, A. Majumder, Department of Mechanical Engineering, Indian Institute of Technology(ISM), Dhanbad 826004, India, H. Dikshit, and Department of Mechanical Engineering, Indian Institute of Technology(ISM), Dhanbad 826004, India. Locomotion Methods of Pipe Climbing robots: A Review. *Journal of Engineering Science and Technology Review*, 11(4):154–165, August 2018.

[10] Thomas Worzyk. *Submarine Power Cables: Design, Installation, Repair, Environmental Aspects*. Springer Science & Business Media, August 2009. Google-Books-ID: X8QfRT_SYDgC.

[11] Charles Spraul, Hong-Duc Pham, Vincent Arnal, and Reynaud Marine. Effect of Marine Growth on Floating Wind Turbines Mooring Lines Responses. In Association Française de Mécanique, editor, *23e Congrès Français de Mécanique*, Congrès français de mécanique, Lille, France, August 2017. AFM, Maison de la Mécanique, 39/41 rue Louis Blanc - 92400 Courbevoie.

[12] Gaosheng Luo, Chuankun Luo, Shimin Gao, Jingxiang Xu, Xuteng Bao, Zhiqiang Ma, and Zhe Jiang. Research on passive adaptive wall-climbing cleaning and inspection robot of marine cylindrical steel structure based on conical magnetic adsorption wheel. *Ocean Engineering*, 314:119676, December 2024.

[13] Claudio Camerini, Miguel Freitas, Ricardo Artigas Langer, Jean Pierre Von Der Weid, and Robson Marnet. Autonomous Underwater Riser Inspection Tool. In *2010 8th International Pipeline Conference, Volume 3*, pages 673–679, Calgary, Alberta, Canada, January 2010. ASMEDC.

[14] Our Technology - Rototech, November 2024.

[15] M. Legg, M. K. Yücel, I. Garcia de Carellan, V. Kappatos, C. Selcuk, and T. H. Gan. Acoustic methods for biofouling control: A review. *Ocean Engineering*, 103:237–247, July 2015.

[16] Bingyin Ma, Tho Nguyen, Michael Corsar, and Matthew Kimball. *Design and control of a robotic system to climb on curved risers to enable pipeline inspection*. January 2019.

[17] Tomonari Yamamoto, Masashi Konyo, Kenjiro Tadakuma, and Satoshi Tadokoro. High-speed sliding-inchworm motion mechanism with expansion-type pneumatic hollow-shaft actuators for in-pipe inspections. *Mechatronics*, 56:101–114, December 2018.

[18] Muhammad Khan, Thirawat Chuthong, Cao Do, Mathias Thor, Peter Billeschou, Jørgen Larsen, and Poramate Manoonpong. iCrawl: An Inchworm-Inspired Crawling Robot. *IEEE Access*, 8:1–1, January

2020.

[19] Jun Shintake, Vito Cacucciolo, Dario Floreano, and Herbert Shea. Soft Robotic Grippers. *Advanced Materials*, 30(29):1707035, 2018. _eprint: https://advanced.onlinelibrary.wiley.com/doi/pdf/10.1002/adma.201707035.

[20] Youngjoo Ahn, Yoonjung Jang, Narayanan Selvapalam, Gyeongwon Yun, and Kimoon Kim. Supramolecular Velcro for Reversible Underwater Adhesion. *Angewandte Chemie International Edition*, 52(11):3140–3144, 2013. _eprint: https://onlinelibrary.wiley.com/doi/pdf/10.1002/anie.201209382.

[21] Xiaoyan Xu, Shifeng Guo, and Gyula Julius Vancso. Perceiving and Countering Marine Biofouling: Structure, Forces, and Processes at Surfaces in Sea Water Across the Length Scales. *Langmuir*, 41(12):7996–8018, April 2025.

[22] Robert E. Smith III. Undersea hydraulic coupling with locking mechanism, May 1999.

[23] Dongpo Zhao and Haitao Wang. Topology Optimization of Compliant Mechanisms Considering Manufacturing Uncertainty, Fatigue, and Static Failure Constraints. *Processes*, 11(10):2914, October 2023.

[24] Jaronie Mohd Jani, Martin Leary, Aleksandar Subic, and Mark A. Gibson. A review of shape memory alloy research, applications and opportunities. *Materials & Design (1980-2015)*, 56:1078–1113, April 2014.

[25] Xianyang Cai and Bin Tang. Self-adaptive bistable gripper with Fin Ray effect for versatile grasping. *International Journal of Mechanical Sciences*, 295:110279, June 2025.

[26] Jiaxin Huang, Jian Shen, Yilin Zheng, Yanbo Guo, and Zhigong Song. A fractal gripper with switchable mode for geometry adaptive manipulation. *Scientific Reports*, 15(1):14657, April 2025.

[27] Daigo Tokunaga, Satoshi Nishikawa, and Kazuo Kiguchi. One-to-Many Tendon Driven System for Robotic Prosthetic Hand. *IEEE Access*, 13:120181–120189, 2025.

[28] Chetan P Chaudhari, Bhushan B Thakare, Saurabh R Patil, and Shrikant U Gunjal. A STUDY OF BEARING AND ITS TYPES. *Vol. No.*, 2015.

[29] S Li, C Wei, and Y Wang. Fabrication and service of all-ceramic ball bearings for extreme conditions applications. *IOP Conference Series: Materials Science and Engineering*, 1009(1):012032, January 2021.

[30] Sanjit S. Chavan. Study of Tweel Non-Pneumatic Tires. *International Journal for Research in Applied Science and Engineering Technology*, 10(1):1047–1051, January 2022.

[31] Jonathan Larsen, Christian Nuñez, Nicholas Simon, and Jessica Smith. Adaptive Beach Walker. *Mechanical Engineering*, June 2014.

A. Components of CRAB

Figure A.1: Aluminium coil

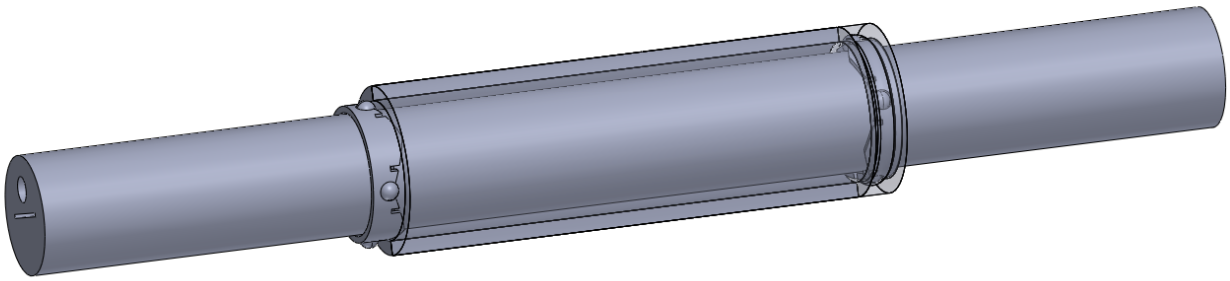

Figure A.2: CAD model of the structural link integrated with the bearing. The left bearing housing is hidden and surrounding components are rendered transparent to reveal the internal assembly.

Figure A.3: Link with bearing

Click to see full view

2 x neodymium magnetic system with rubber Ø 66 mm thread (male thread) M8 - adhesive force 25 kg - 2 pieces - strong magnets with rubber coating anti-slip coating

Brand: Magnosphere

4.8 ★★★★★ (7) | Search this page

€17[54]

All prices include VAT.

Material	Neodymium
Brand	Magnosphere
Product dimensions	24L x 66W x 24Th millimetres
Colour	Black
Shape	Cylindrical
Item thickness	8.5 Millimetres
Number of pieces	2

See more

About this item

- Quantity: 2 pieces - diameter (D): Ø 66 mm - total height (H): 23.5 mm - thread (m): M8 - plate height (h1): 8.5 mm - screw length (H2): 15 mm - operating temperature: max. 80 °C - adhesive force: max. Approx. 25kg
- Strong adhesive force: Our rubber threaded neodymium magnets hold an impressive 55 kg and provide a reliable mounting solution for car lights, cameras, tools and more
- Protection and non-slip – thanks to the rubber surface, our magnets provide effective protection against scratches and damage. The non-slip coating ensures a secure grip, even on smooth surfaces
- Versatile uses: ideal for use in vehicles, motorhomes, workshops and outdoors. Easily mount lights, doorbells, solar lights and more with these high-quality magnet systems
- Easy installation: The magnets have threaded sockets in sizes M4 to M8 and can be easily screwed on and mounted. Perfect for quick and secure fixings without drilling or gluing
- High quality and precision: our magnets are made of high-quality neodymium and are precisely made. The rubber surface ensures gentle use and prevents damage to sensitive surfaces
- Durable and corrosion-resistant: with a triple anti-corrosion coating and the waterproof rubber coating surface, our magnets offer high resistance to external influences. Suitable for long-term indoor and outdoor use

Figure A.4: Big magnet

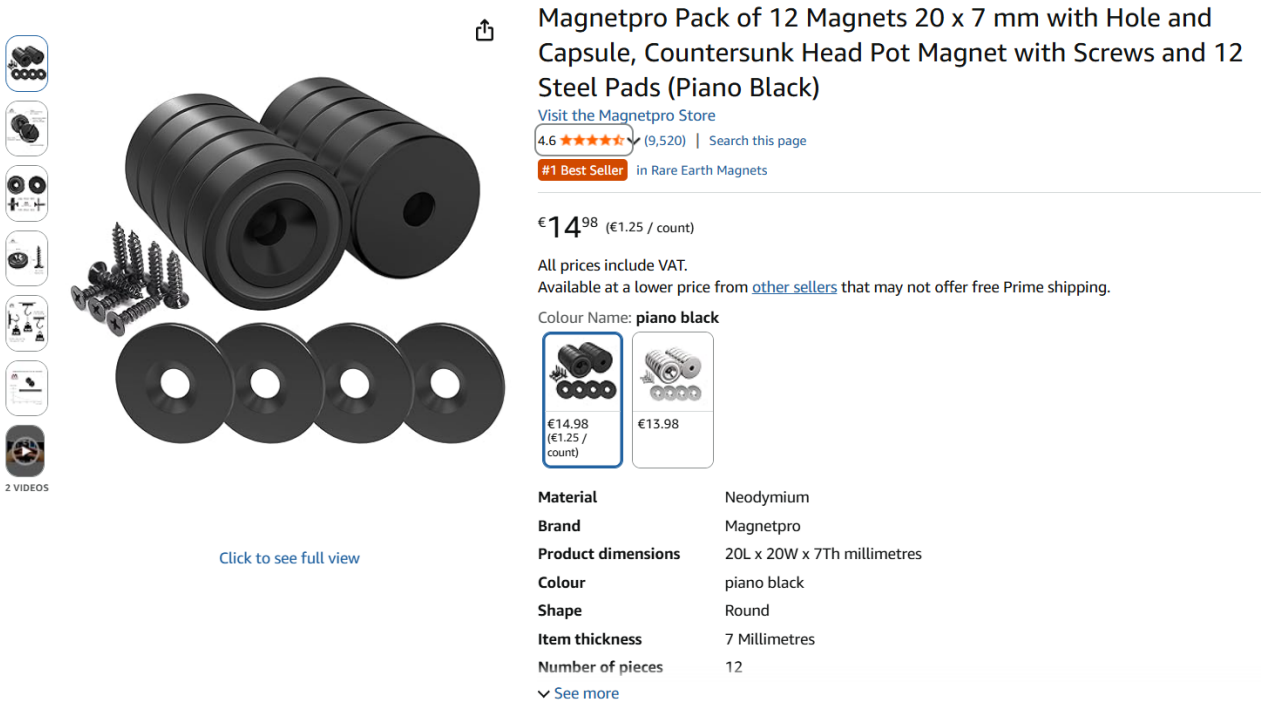

Figure A.5: Small magnets

B. Fabrication of the flexible wheel

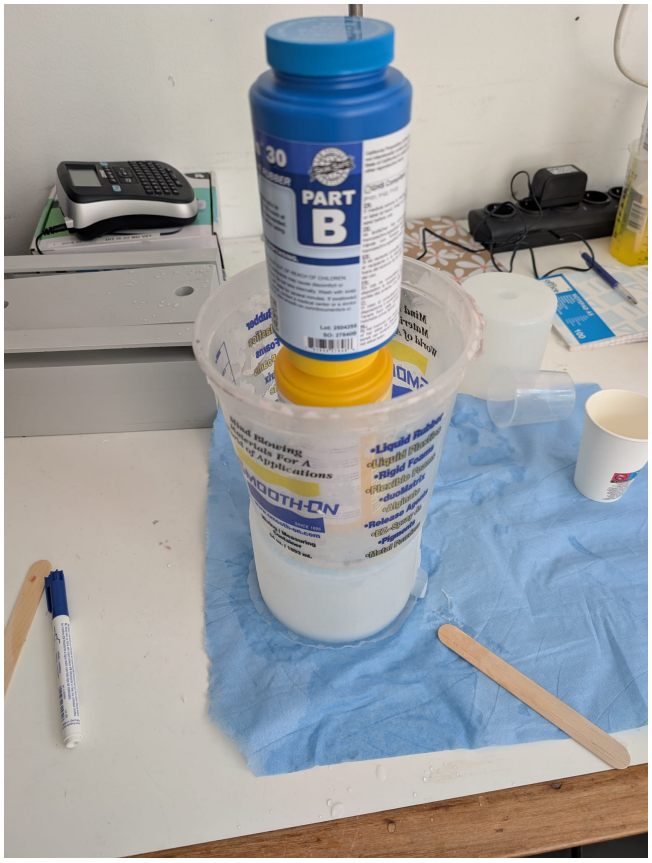

Figure B.1: Joining top and bottem of the wheel, with bottles as weights to ensure proper sealing.

C. Empirical setup

(a) Stiffness measurement

Displacement	Measurements stiffness (N)
10	18
20	29
30	40
Displacement	Measurements friction (N)
10	5
20	11
30	22

Figure C.2: Test setup results

Displacement	Measurements stiffness (N)	C10=0.15 C01=0.04	C10=0.25 C01=0.03	C10=0.23 C01=0.03	C10=0.3 C01=0.04
10	13	2	1	1	2
20	29	7	18	17	22
30	40	21	39	36	45
Displacement	Measurements friction (N)	C10=0.3 Fc=0.5	C10=0.3 Fc=0.8		
10	5	1	2		
20	11	5	7		
30	16	13	16		

Figure C.3: Model calibration to fit test setup results

D. First iteration CRAB prototype

The first iteration was printed with 2 layer thickness PLA. Because of strength concerns, test where conducted in water, however it still broke.

Figure D.1: Open gripper

(a) Closed gripper

(b) Fully closed gripper

Figure D.2: Comparison of the gripper in the closed and fully closed positions.

Figure D.3: CRAB in water.

Figure D.4: Breaking point (with unsuccessful duct tape as a solution)